

REDUCING THE SPECTRAL INDEX IN F-TERM HYBRID INFLATION

C. PALLIS

*School of Physics and Astronomy,
The University of Manchester,
Manchester M13 9PL,
UNITED KINGDOM
kpallis@auth.gr*

October 28, 2018

ABSTRACT

We consider a class of well motivated supersymmetric models of F-term hybrid inflation (FHI) which can be linked to the supersymmetric grand unification. The predicted scalar spectral index n_s cannot be smaller than 0.97 and can exceed unity including corrections from minimal supergravity, if the number of e-foldings corresponding to the pivot scale $k_* = 0.002/\text{Mpc}$ is around 50. These results are marginally consistent with the fitting of the three-year Wilkinson microwave anisotropy probe data by the standard power-law cosmological model with cold dark matter and a cosmological constant. However, n_s can be reduced by applying two mechanisms: (i) The utilization of a quasi-canonical Kähler potential with a convenient choice of a sign and (ii) the restriction of the number of e-foldings that k_* suffered during FHI. In the case (i), we investigate the possible reduction of n_s without generating maxima and minima of the potential on the inflationary path. In the case (ii), the additional e-foldings required for solving the horizon and flatness problems can be generated by a subsequent stage of fast-roll [slow-roll] modular inflation realized by a string modulus which does [does not] acquire effective mass before the onset of modular inflation.

1 INTRODUCTION

A plethora of precise cosmological observations on the *cosmic microwave background radiation* (CMB) and the large-scale structure in the universe has strongly favored the idea of inflation [1] (for reviews see e.g. Refs. [2, 3, 4]). We focus on a set of well-motivated, popular and quite natural models [5] of *supersymmetric* (SUSY) *F-term hybrid inflation* (FHI) [6], realized [7] at (or very close to) the SUSY *grand unified theory* (GUT) scale $M_{\text{GUT}} = 2.86 \times 10^{16}$ GeV. Namely, we consider the standard [7], shifted [8] and smooth [9] FHI. In the context of global SUSY (and under the assumption that the problems of the *standard big bag cosmology* (SBB) are resolved exclusively by FHI), these models predict scalar spectral index, n_s , extremely close to unity and without much running, a_s . Moreover, corrections induced by *minimal supergravity* (mSUGRA) drive [10] n_s closer to unity or even upper than it.

These predictions are marginally consistent with the fitting of the three-year *Wilkinson microwave anisotropy probe* (WMAP3) results by the standard power-law cosmological model with cold dark matter and a cosmological constant (Λ CDM). Indeed, one obtains [11] that, at the pivot scale $k_* = 0.002/\text{Mpc}$, n_s is to satisfy the following rather narrow range of values:

$$n_s = 0.958 \pm 0.016 \Rightarrow 0.926 \lesssim n_s \lesssim 0.99 \quad (1)$$

at 95% confidence level with negligible a_s .

A possible resolution of the tension between FHI and the data is suggested in Ref. [12]. There, it is argued that values of n_s between 0.98 and 1 can be made to be compatible with the data by taking into account a sub-dominant contribution to the curvature perturbation in the universe due to cosmic strings which may be (but are not necessarily [13]) formed during the phase transition at the end of FHI. However, in such a case, the GUT scale is constrained to values well below M_{GUT} [14, 15, 16]. In the following, we reconsider two other resolutions of the problem above without the existence of cosmic strings:

- (i) FHI within *quasi-canonical SUGRA* (qSUGRA). In this scenario, we invoke [16, 17] a departure from mSUGRA, utilizing a quasi-canonical (we use the term coined originally in Ref. [18]) Kähler potential with a convenient arrangement of the sign of the next-to-minimal term. This yields a negative mass term for the inflaton in the inflationary potential which can lead to acceptable n_s 's. In a sizable portion of the region in Eq. (1) a local minimum and maximum appear in the inflationary trajectory, thereby jeopardizing the attainment of FHI. In that case, we are obliged to assume suitable initial conditions, so that hilltop inflation [19] takes place as the inflaton rolls from the maximum down to smaller values. Therefore, n_s can become consistent with Eq. (1) but only at the cost of a mild tuning [16] of the initial conditions. On the other hand, we can show [20, 21] that acceptable n_s 's can be obtained even without this minimum-maximum problem.
- (ii) FHI followed by *modular inflation* (MI). It is recently proposed [22] that a two-step inflationary set-up can allow acceptable n_s 's in the context of FHI models even with

canonical Kähler potential. The idea is to constrain the number of e-foldings that k_* suffers during FHI to relatively small values, which reduces n_s to acceptable values. The additional number of e-foldings required for solving the horizon and flatness problems of SBB can be obtained by a second stage of inflation (named [22] complementary inflation) implemented at a lower scale. We can show that MI [23] (for another possibility see Ref. [24]), realized by a string modulus, can play successfully the role of complementary inflation. A key issue of this set-up is the evolution of the modulus before the onset of MI [25, 26]. We single out two cases according to whether or not the modulus acquires effective mass before the commencement of MI. We show that, in the first case, MI is of the slow-roll type and a very mild tuning of the initial value of the modulus is needed in order to obtain solution compatible with a number of constraints. In the second case, the initial value of the modulus can be predicted due to its evolution before MI, and MI turns out to be of the fast-roll [27] type. However, in our minimal set-up, an upper bound on the total number of e-foldings obtained during FHI emerges, which signalizes a new disturbing tuning. Possible ways out of this situation are also proposed.

In this presentation we reexamine the above ideas for the reduction of n_s within FHI, implementing the following improvements:

- In the case (i) we delineate the parametric space of the FHI models with acceptable n_s 's maintaining the monotonicity of the inflationary potential and derive analytical expressions which approach fairly our numerical results.
- In the case (ii) we incorporate the *nucleosynthesis* (NS) constraint and we analyze the situation in which the inflaton of MI acquires mass before the onset of MI, under some simplified assumptions [28].

The text is organized as follows: In Sec. 2, we review the basic FHI models and in the following we present the two methods for the reduction of n_s using qSUGRA (Sec. 3) or constructing a two-step inflationary scenario (Sec. 4). Our conclusions are summarized in Sec. 5.

2 THE FHI MODELS

We outline the salient features (the superpotential in Sec 2.1, the SUSY potential in Sec. 2.2 and the inflationary potential in Sec. 2.3) of the basic types of FHI and we present their predictions in Sec. 2.6, calculating a number of observable quantities introduced in Sec. 2.4, within the standard cosmological set-up described in Sec. 2.5.

2.1 THE RELEVANT SUPERPOTENTIAL

The F-term hybrid inflation can be realized [5] adopting one of the superpotentials below:

$$W = \begin{cases} \kappa S (\bar{\Phi}\Phi - M^2) & \text{for standard FHI,} \\ \kappa S (\bar{\Phi}\Phi - M^2) - S \frac{(\bar{\Phi}\Phi)^2}{M_S^2} & \text{for shifted FHI,} \\ S \left(\frac{(\bar{\Phi}\Phi)^2}{M_S^2} - \mu_S^2 \right) & \text{for smooth FHI,} \end{cases} \quad \text{where} \quad (2)$$

- S is a left handed superfield, singlet under a GUT gauge group G ,
- $\bar{\Phi}, \Phi$ is a pair of left handed superfields belonging to non-trivial conjugate representations of G , and reducing its rank by their *vacuum expectation values* (v.e.vs),
- $M_S \sim 5 \times 10^{17}$ GeV is an effective cutoff scale comparable with the string scale,
- κ and M, μ_S ($\sim M_{\text{GUT}}$) are parameters which can be made positive by field redefinitions.

The superpotential in Eq. (2) for standard FHI is the most general renormalizable superpotential consistent with a continuous R-symmetry [7] under which

$$S \rightarrow e^{i\alpha} S, \quad \bar{\Phi}\Phi \rightarrow \bar{\Phi}\Phi, \quad W \rightarrow e^{i\alpha} W. \quad (3)$$

Including in this superpotential the leading non-renormalizable term, one obtains the superpotential of shifted [8] FHI in Eq. (2). Finally, the superpotential of smooth [9] FHI can be produced if we impose an extra Z_2 symmetry under which $\Phi \rightarrow -\Phi$ and, therefore, only even powers of the combination $\bar{\Phi}\Phi$ can be allowed.

2.2 THE SUSY POTENTIAL

The SUSY potential, V_{SUSY} , extracted (see e.g. ref. [2]) from W in Eq. (2) includes F and D-term contributions. Namely,

$$V_{\text{SUSY}} = V_{\text{F}} + V_{\text{D}}, \quad \text{where}$$

- The F-term contribution can be written as:

$$V_{\text{F}} = \begin{cases} \kappa^2 M^4 ((\Phi^2 - 1)^2 + 2S^2 \Phi^2) & \text{for standard FHI,} \\ \kappa^2 M^4 ((\Phi^2 - 1 - \xi \Phi^4)^2 + 2S^2 \Phi^2 (1 - 2\xi \Phi^2)^2) & \text{for shifted FHI,} \\ \mu_S^4 ((1 - \Phi^4)^2 + 16S^2 \Phi^6) & \text{for smooth FHI,} \end{cases} \quad (4)$$

where the scalar components of the superfields are denoted by the same symbols as the corresponding superfields and

$$\begin{cases} \Phi = |\Phi|/M \quad \text{and} \quad S = |S|/M & \text{for standard or shifted FHI,} \\ \Phi = |\Phi|/2\sqrt{\mu_S M_S} \quad \text{and} \quad S = |S|/\sqrt{2\mu_S M_S} & \text{for smooth FHI,} \end{cases}$$

with $\xi = M^2/\kappa M_S$ and $1/7.2 < \xi < 1/4$ [8].

In Figs. 1, 2 and 3 we present the three dimensional plot of V_F versus $\pm\Phi$ and S for standard, shifted and smooth FHI, respectively. The inflationary trajectories are also depicted by bold points, whereas the critical points by red/light points.

- The D-term contribution V_D vanishes for $|\bar{\Phi}| = |\Phi|$.

Using the derived V_{SUSY} , we can understand that W in Eq. (2) plays a twofold crucial role:

- It leads to the spontaneous breaking of G . Indeed, the vanishing of V_F gives the v.e.vs of the fields in the SUSY vacuum. Namely,

$$\langle S \rangle = 0 \text{ and } |\langle \bar{\Phi} \rangle| = |\langle \Phi \rangle| = v_G = \begin{cases} M & \text{for standard FHI,} \\ \frac{M\sqrt{1-\sqrt{1-4\xi}}}{\sqrt{2\xi}} & \text{for shifted FHI,} \\ \sqrt{\mu_S M_S} & \text{for smooth FHI} \end{cases} \quad (5)$$

(in the case where $\bar{\Phi}$, Φ are not *Standard Model* (SM) singlets, $\langle \bar{\Phi} \rangle$, $\langle \Phi \rangle$ stand for the v.e.vs of their SM singlet directions). The non-zero value of the v.e.v v_G signalizes the spontaneous breaking of G .

- It gives also rise to FHI. This is due to the fact that, for large enough values of $|S|$, there exist valleys of local minima of the classical potential with constant (or almost constant in the case of smooth FHI) values of V_F . In particular, we can observe that $V_F = \text{cst}$ along the following F-flat direction(s):

$$\begin{aligned} \Phi &= 0 && \text{for standard FHI,} \\ \Phi &= 0 \text{ Or } \Phi = \sqrt{1/2\xi} && \text{for shifted FHI,} \\ \Phi &= 0 \text{ Or } \Phi = 1/2\sqrt{6S} && \text{for smooth FHI.} \end{aligned}$$

From Figs. 1-3 we deduce that the flat direction $\Phi = 0$ corresponds to a minimum of V_F , for $|S| \gg M$, in the cases of standard and shifted FHI and to a maximum of V_F in the case of smooth FHI. Since FHI can be attained along a minimum of V_F we infer that, during standard FHI, the GUT gauge group G is necessarily restored. As a consequence, topological defects such as strings [14, 15, 16], monopoles, or domain walls may be produced [9] via the Kibble mechanism [30] during the spontaneous breaking of G at the end of FHI. This can be avoided in the other two cases, since the form of V_F allows for non-trivial inflationary valleys along which G is spontaneously broken (since the waterfall fields $\bar{\Phi}$ and Φ can acquire non-zero values during FHI). Therefore, no topological defects are produced in these cases. In Table 1 we shortly summarize comparatively the key features of the various versions of FHI.

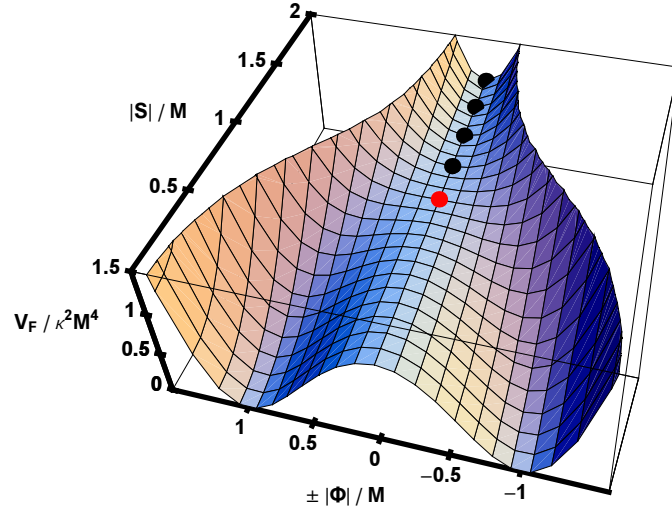


FIGURE 1: The three dimensional plot of the (dimensionless) F-term potential $V_F/\kappa^2 M^4$ for standard FHI versus $S = |S|/M$ and $\pm \Phi = \pm|\Phi|/M$. The inflationary trajectory is also depicted by black points whereas the critical point by a red/light point.

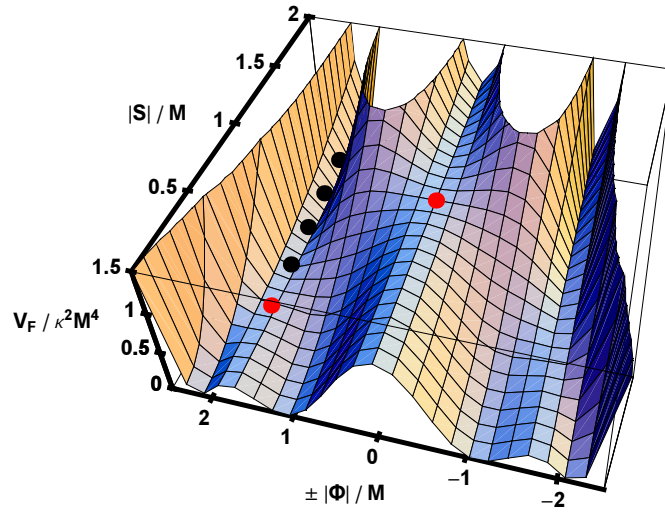


FIGURE 2: The three dimensional plot of the (dimensionless) F-term potential $V_F/\kappa^2 M^4$ for shifted FHI versus $S = |S|/M$ and $\pm \Phi = \pm|\Phi|/M$ for $\xi = 1/6$. The (shifted) inflationary trajectory is also depicted by black points whereas the critical points (of the shifted and standard trajectories) are depicted by red/light points.

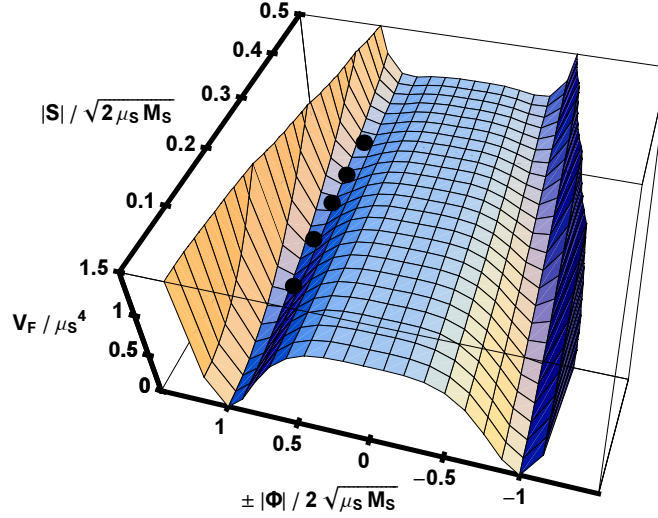


FIGURE 3: The three dimensional plot of the (dimensionless) F-term potential V_F / μ_S^4 for smooth FHI versus $S = |S| / \sqrt{2\mu_S M_S}$ and $\pm \Phi = \pm |\Phi| / 2\sqrt{\mu_S M_S}$. The inflationary trajectory is also depicted by black points.

2.3 THE INFLATIONARY POTENTIAL

The general form of the potential which can drive the various versions of FHI reads

$$V_{\text{HI}} = V_{\text{HI0}} + V_{\text{HIc}} + V_{\text{HIS}} + V_{\text{HIT}}, \quad \text{where:} \quad (6)$$

- V_{HI0} is the dominant (constant) contribution to V_{HI} , which can be written as follows:

$$V_{\text{HI0}} = \begin{cases} \kappa^2 M^4 & \text{for standard FHI,} \\ \kappa^2 M_\xi^4 & \text{for shifted FHI,} \\ \mu_S^4 & \text{for smooth FHI,} \end{cases} \quad (7)$$

with $M_\xi = M \sqrt{1/4\xi - 1}$.

- V_{HIc} is the contribution to V_{HI} which generates a slope along the inflationary valley for driving the inflaton towards the vacua. In the cases of standard [7] and shifted [8] FHI, this slope can be generated by the SUSY breaking on this valley. Indeed, $V_{\text{HI0}} > 0$ breaks SUSY and gives rise to logarithmic radiative corrections to the potential originating from a mass splitting in the $\Phi - \bar{\Phi}$ supermultiplets. On the other hand, in the case of smooth [9] FHI, the inflationary valleys are not classically flat and, thus, there is no need of radiative corrections. Introducing the canonically normalized inflaton field $\sigma = \sqrt{2}|S|$, V_{HIc} can be written as follows:

	TYPES OF FHI		
	STANDARD	SHIFTED	SMOOTH
The $\Phi = 0$ F-flat direction is:	Minimum for $ S \gg M$	Minimum for $ S \gg M$	Maximum
Critical point along the inflationary path?	Yes ($\sigma_c = \sqrt{2}M$)	Yes ($\sigma_c = M_\xi$)	No
Classical flatness of the inflationary path?	Yes	Yes	No
Topological defects?	Yes	No	No

TABLE 1: Differences and similarities of the various types of FHI.

$$V_{\text{HIc}} = \begin{cases} \frac{\kappa^4 M^4 N}{32\pi^2} \left(2 \ln \frac{\kappa^2 x M^2}{Q^2} + f_c(x) \right) & \text{for standard FHI,} \\ \frac{\kappa^4 M_\xi^4}{16\pi^2} \left(2 \ln \frac{\kappa^2 x_\xi M_\xi^2}{Q^2} + f_c(x_\xi) \right) & \text{for shifted FHI,} \\ -2\mu_s^6 M_S^2 / 27\sigma^4 & \text{for smooth FHI,} \end{cases} \quad (8)$$

with $f_c(x) = (x+1)^2 \ln(1+1/x) + (x-1)^2 \ln(1-1/x) \Rightarrow f_c(x) \simeq 3$ for $x \gg 1$, $x = \sigma^2/2M^2$ and $x_\xi = \sigma^2/M_\xi^2$. Also N is the dimensionality of the representations to which $\bar{\Phi}$ and Φ belong and Q is a renormalization scale. Although, in some parts (see Sec. 4.3) of our work, rather large κ 's are used for standard and shifted FHI, renormalization group effects [31] remain negligible.

In our numerical applications in Secs. 2.6, 3.3, and 4.3 we take $N = 2$ for standard FHI. This corresponds to the left-right symmetric GUT gauge group $SU(3)_c \times SU(2)_L \times SU(2)_R \times U(1)_{B-L}$ with $\bar{\Phi}$ and Φ belonging to $SU(2)_R$ doublets with $B-L = -1$ and 1 respectively. It is known [13] that no cosmic strings are produced during this realization of standard FHI. As a consequence, we are not obliged to impose extra restrictions on the parameters (as e.g. in Refs. [15, 14]). Let us mention, in passing, that, in the case of shifted [8] FHI, the GUT gauge group is the Pati-Salam group $SU(4)_c \times SU(2)_L \times SU(2)_R$. Needless to say that the case of smooth FHI is independent on the adopted GUT since the inclination of the inflationary path is generated at the classical level and the addition of any radiative correction is expected to be subdominant.

- V_{HIS} is the SUGRA correction to V_{HI} . This emerges if we substitute a specific choice for the Kähler potential K into the SUGRA scalar potential which (without the D-terms) is given by

$$V_{\text{SUGRA}} = e^{K/m_{\text{P}}^2} \left[(F_i)^* K^{i^*j} F_j - 3 \frac{|W|^2}{m_{\text{P}}^2} \right], \quad (9)$$

where $F_i = W_i + K_i W/m_{\text{P}}^2$, a subscript i [i^*] denotes derivation *with respect to* (w.r.t) the complex scalar field ϕ^i [ϕ^{i^*}] and K^{i^*j} is the inverse of the matrix K_{ji^*} . The most elegant, restrictive and highly predictive version of FHI can be obtained, assuming minimal Kähler potential [6, 10], $K_{\text{m}} = |S|^2$. In such a case V_{HIS} becomes

$$V_{\text{HISm}} = V_{\text{HI0}} \frac{\sigma^4}{8m_{\text{P}}^4}, \quad (10)$$

where $m_{\text{P}} \simeq 2.44 \times 10^{18}$ GeV is the reduced Planck scale. We can observe that in this case, no other free parameter is added to the initial set of the free parameters of each model (see Sec. 2.6).

- V_{HIT} is the most important contribution to V_{HI} from the soft SUSY effects [14, 16, 32] which can be uniformly parameterized as follows:

$$V_{\text{HIT}} = a_{\text{S}} \sqrt{V_{\text{HI0}}} \sigma / \sqrt{2} \quad (11)$$

where a_{S} is of the order of 1 TeV. V_{HIT} starts [14, 16, 32] playing an important role in the case of standard FHI for $\kappa \lesssim 5 \times 10^{-4}$ and does not have [32], in general, any significant effect in the cases of shifted and smooth FHI.

2.4 INFLATIONARY OBSERVABLES

Under the assumption that (i) possible deviation from mSUGRA is suppressed (see Sec. 3.2) and (ii) the cosmological scales leave the horizon during FHI and are not reprocessed during a possible subsequent inflationary stage (see Sec. 4), we can apply the standard (see e.g. Refs. [2, 3, 4]) calculations for the inflationary observables of FHI. Namely, we can find:

- The number of e-foldings N_{HI^*} that the scale k_* suffers during FHI,

$$N_{\text{HI}^*} = \frac{1}{m_{\text{P}}^2} \int_{\sigma_{\text{f}}}^{\sigma_*} d\sigma \frac{V_{\text{HI}}}{V'_{\text{HI}}}, \quad (12)$$

where the prime denotes derivation w.r.t σ , σ_* is the value of σ when the scale k_* crosses outside the horizon of FHI, and σ_{f} is the value of σ at the end of FHI, which can be found, in the slow roll approximation, from the condition

$$\max\{\epsilon(\sigma_{\text{f}}), |\eta(\sigma_{\text{f}})|\} = 1, \quad \text{where } \epsilon \simeq \frac{m_{\text{P}}^2}{2} \left(\frac{V'_{\text{HI}}}{V_{\text{HI}}} \right)^2 \quad \text{and } \eta \simeq m_{\text{P}}^2 \frac{V''_{\text{HI}}}{V_{\text{HI}}}. \quad (13)$$

In the cases of standard [7] and shifted [8] FHI and in the parameter space where the terms in Eq. (10) do not play an important role, the end of inflation coincides with the onset of the GUT phase transition, i.e. the slow roll conditions are violated close to the critical point $\sigma_{\text{c}} = \sqrt{2}M$ [$\sigma_{\text{c}} = M_{\xi}$] for standard [shifted] FHI, where the waterfall regime commences. On the contrary, the end of smooth [9] FHI is not abrupt since the inflationary path is stable w.r.t $\Phi - \bar{\Phi}$ for all σ 's and σ_{f} is found from Eq. (13).

- The power spectrum $P_{\mathcal{R}}$ of the curvature perturbations generated by σ at the pivot scale k_*

$$P_{\mathcal{R}*}^{1/2} = \frac{1}{2\sqrt{3}\pi m_{\text{P}}^3} \left. \frac{V_{\text{HI}}^{3/2}}{|V'_{\text{HI}}|} \right|_{\sigma=\sigma_*}. \quad (14)$$

- The spectral index

$$n_s = 1 + \left. \frac{d \ln P_{\mathcal{R}}}{d \ln k} \right|_{\sigma=\sigma_*} = 1 - m_{\text{P}}^2 \left. \frac{V'_{\text{HI}}}{V_{\text{HI}}} (\ln P_{\mathcal{R}})' \right|_{\sigma=\sigma_*} = 1 - 6\epsilon_* + 2\eta_*, \quad (15)$$

and its running

$$\alpha_s = \left. \frac{d^2 \ln P_{\mathcal{R}}}{d \ln k^2} \right|_{\sigma=\sigma_*} = \frac{2}{3} (4\eta_*^2 - (n_s - 1)^2) - 2\xi_*, \quad (16)$$

where $\xi \simeq m_{\text{P}}^4 V_{\text{HI}}' V_{\text{HI}}''' / V_{\text{HI}}^2$, the variables with subscript $*$ are evaluated at $\sigma = \sigma_*$ and we have used the identity $d \ln k = H dt = -d\sigma / \sqrt{2\epsilon} m_{\text{P}}$.

We can obtain a rather accurate estimation of the expected n_s 's if we calculate analytically the integral in Eq. (12) and solve the resulting equation w.r.t σ_* . We pose $\sigma_f = \sigma_c$ for standard and shifted FHI whereas we solve the equation $\eta(\sigma_f) = 1$ for smooth FHI ignoring V_{HIS} . Taking into account that $\epsilon < \eta$ we can extract n_s from Eq. (15). In the case of global SUSY – setting $V_{\text{HIS}} = V_{\text{HIT}} = 0$ in Eq. (6) – we find

$$n_s = \begin{cases} 1 - 1/N_{\text{HI}*} & \text{for standard and shifted FHI,} \\ 1 - 5/3N_{\text{HI}*} & \text{for smooth FHI,} \end{cases} \quad (17)$$

whereas in the context of mSUGRA – setting $V_{\text{HIS}} = V_{\text{HISm}}$ in Eq. (6) – we find

$$n_s = \begin{cases} 1 - 1/N_{\text{HI}*} + 3k^2 N_{\text{HI}*} / 4\pi^2 & \text{for standard FHI,} \\ 1 - 1/N_{\text{HI}*} + 3k^2 N_{\text{HI}*} / 2\pi^2 & \text{for shifted FHI,} \\ 1 - 5/3N_{\text{HI}*} + 2(6\mu_{\text{S}}^2 M_{\text{S}}^2 N_{\text{HI}*} / m_{\text{P}}^4)^{1/3} & \text{for smooth FHI.} \end{cases} \quad (18)$$

Comparing the expressions of Eq. (17) and (18), we can easily infer that mSUGRA elevates significantly n_s for relatively large k or M_{S} .

2.5 OBSERVATIONAL CONSTRAINTS

Under the assumption that (i) the contribution in Eq. (14) is solely responsible for the observed curvature perturbation (for an alternative scenario see Ref. [33]) and (ii) there is a conventional cosmological evolution after FHI (see point (ii) below), the parameters of the FHI models can be restricted imposing the following requirements:

- (i) The power spectrum of the curvature perturbations in Eq. (14) is to be confronted with the WMAP3 data [11]:

$$P_{\mathcal{R}*}^{1/2} \simeq 4.86 \times 10^{-5} \text{ at } k_* = 0.002/\text{Mpc}. \quad (19)$$

(ii) The number of e-foldings N_{tot} required for solving the horizon and flatness problems of SBB is produced exclusively during FHI and is given by

$$N_{\text{tot}} = N_{\text{HI}^*} \simeq 22.6 + \frac{2}{3} \ln \frac{V_{\text{HI0}}^{1/4}}{1 \text{ GeV}} + \frac{1}{3} \ln \frac{T_{\text{Hrh}}}{1 \text{ GeV}}, \quad (20)$$

where T_{Hrh} is the reheat temperature after the completion of the FHI.

Indeed, the number of e-foldings N_k between horizon crossing of the observationally relevant mode k and the end of inflation can be found as follows [2]:

$$\begin{aligned} \frac{k}{H_0 R_0} = \frac{H_k R_k}{H_0 R_0} &= \frac{H_k}{H_0} \frac{R_k}{R_{\text{Hf}}} \frac{R_{\text{Hf}}}{R_{\text{Hrh}}} \frac{R_{\text{Hrh}}}{R_{\text{eq}}} \frac{R_{\text{eq}}}{R_0} \\ &= \sqrt{\frac{V_{\text{HI0}}}{\rho_{\text{c0}}}} e^{-N_k} \left(\frac{V_{\text{HI0}}}{\rho_{\text{Hrh}}} \right)^{-1/3} \left(\frac{\rho_{\text{Hrh}}}{\rho_{\text{eq}}} \right)^{-1/4} \left(\frac{\rho_{\text{eq}}}{\rho_{\text{m0}}} \right)^{-1/3} \\ \Rightarrow N_k &\simeq \ln \frac{H_0 R_0}{k} + 24.72 + \frac{2}{3} \ln \frac{V_{\text{HI0}}^{1/4}}{1 \text{ GeV}} + \frac{1}{3} \ln \frac{T_{\text{Hrh}}}{1 \text{ GeV}}. \quad (21) \end{aligned}$$

Here, R is the scale factor, $H = \dot{R}/R$ is the Hubble rate, ρ is the energy density and the subscripts 0, k , Hf, Hrh, eq and m denote values at the present (except for the symbols V_{HI0} and $H_{\text{HI0}} = \sqrt{V_{\text{HI0}}}/\sqrt{3}m_{\text{P}}$), at the horizon crossing ($k = R_k H_k$) of the mode k , at the end of FHI, at the end of reheating, at the radiation-matter equidensity point and at the *matter domination* (MD). In our calculation we take into account that $R \propto \rho^{-1/3}$ for *decaying-particle domination* (DPD) or MD and $R \propto \rho^{-1/4}$ for *radiation domination* (RD). We use the following numerical values:

$$\begin{aligned} \rho_{\text{c0}} &= 8.099 \times 10^{-47} h_0^2 \text{ GeV}^4 \quad \text{with } h_0 = 0.71, \\ \rho_{\text{Hrh}} &= \frac{\pi^2}{30} g_{\rho^*} T_{\text{Hrh}}^4 \quad \text{with } g_{\rho^*} = 228.75, \\ \rho_{\text{eq}} &= 2\Omega_{\text{m0}}(1 - z_{\text{eq}})^3 \rho_{\text{c0}} \quad \text{with } \Omega_{\text{m0}} = 0.26 \quad \text{and } z_{\text{eq}} = 3135. \quad (22) \end{aligned}$$

Setting $H_0 = 2.37 \times 10^{-4}/\text{Mpc}$ and $k/R_0 = 0.002/\text{Mpc}$ in Eq. (21) we derive Eq. (20).

The cosmological evolution followed in the derivation of Eq. (20) is demonstrated in Fig. 4 where we design the (dimensionless) physical length $\bar{\lambda}_{\text{H0}} = \lambda_{\text{H0}}/R_0$ (dotted line) corresponding to our present particle horizon and the (dimensionless) particle horizon $\bar{R}_H = 1/\bar{H} = H_0/H$ (solid line) versus the logarithmic time $\tau = \ln R/R_0$. We use $V_{\text{HI0}}^{1/4} = 10^{15} \text{ GeV}$ and $T_{\text{Hrh}} = 10^9 \text{ GeV}$ (which result to $N_{\text{HI}^*} \simeq 55$). We take into account that $\ln \bar{\lambda} \propto \tau$, $\bar{R}_H = H_0/H_{\text{HI0}}$ for FHI and $\ln \bar{R}_H \propto 2\tau$ [$\ln \bar{R}_H \propto 1.5\tau$] for RD [MD]. The various eras of the cosmological evolution are also clearly shown.

Fig. 4 visualizes [4] the resolution of the horizon problem of SBB with the use of FHI. Indeed, suppose that $\bar{\lambda}_{\text{H0}}$ (which crosses the horizon today, $\bar{\lambda}_{\text{H0}}(0) = \bar{R}_H(0)$) indicates the distance between two photons we detect in CMB. In the absence of FHI, the observed homogeneity of CMB remains unexplained since λ_{H0} was outside the horizon, $(\bar{\lambda}_{\text{H0}}/\bar{R}_H)(\tau_{\text{LS}}) \simeq 33.11$, at the time of *last-scattering* (LS) (with temperature $T_{\text{LS}} \simeq$

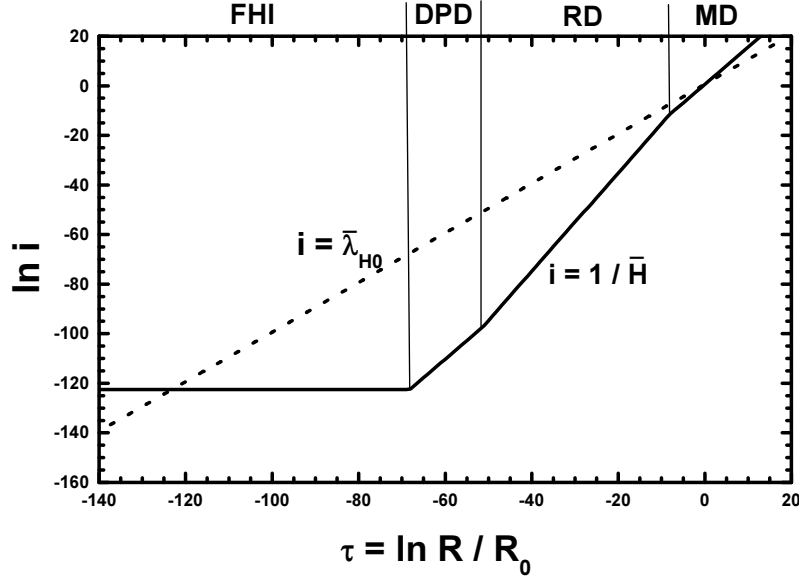


FIGURE 4: The evolution of the quantities $1/\bar{H} = H/H_0$ with (solid line) and $\bar{\lambda}_{H0} = \lambda/R_0$ (dotted line) as a function of τ for $V_{H10}^{1/4} = 10^{15}$ GeV, $N_{H1*} \simeq 55$ and $T_{Hrh} = 10^9$ GeV. The various eras of the cosmological evolution are also shown.

0.26 eV or logarithmic time $\tau_{LS} \simeq -7$) when the two photons were emitted and so, they could not establish thermodynamic equilibrium. There were 3.6×10^4 disconnected regions within the volume $\bar{\lambda}_{H0}^3(\tau_{LS})$. In other words, photons on the LS surface (with radius $\bar{R}_H(0)$) separated by an angle larger than $\theta = \bar{\lambda}_{LS}(0)/\bar{R}_H(0) \simeq (1/33.11)$ rad = 1.7^0 were not in casual contact – here, λ_{LS} is the physical length which crossed the horizon at LS. On the contrary, in the presence of FHI, λ_{H0} has a chance to be within the horizon again, $\bar{\lambda}_{H0} < \bar{R}_H$, if FHI produces around 56 e-foldings before its termination. If this happens, the homogeneity and the isotropy of CMB can be easily explained: photons that we receive today and were emitted from causally disconnected regions of the LS surface, have the same temperature because they had a chance to communicate to each other before FHI.

2.6 NUMERICAL RESULTS

Our numerical investigation depends on the parameters:

$$\sigma_*, v_G \text{ and } \begin{cases} \kappa & \text{for standard FHI,} \\ \kappa \text{ with fixed } M_S = 5 \times 10^{17} \text{ GeV} & \text{for shifted FHI,} \\ M_S & \text{for smooth FHI.} \end{cases}$$

In our computation, we use as input parameters κ or M_S and σ_* and we then restrict v_G and σ_* so as Eqs. (19) and (20) are fulfilled. Using Eqs. (15) and (16) we can extract n_s and α_s

SHIFTED FHI			SMOOTH FHI		
	WITHOUT	WITH		WITHOUT	WITH
	mSUGRA			mSUGRA	
$\kappa/10^{-3}$	9.2		$M_S/5 \times 10^{17}$ GeV	1.56	0.79
$\sigma_*/10^{16}$ GeV	5.37		$\sigma_*/10^{16}$ GeV	26.8	32.9
$M/10^{16}$ GeV	2.3		$\mu_S/10^{16}$ GeV	0.1	0.21
$1/\xi$	4.36		$\sigma_f/10^{16}$ GeV	13.4	13.4
$N_{\text{HI}*}$	52.2		$N_{\text{HI}*}$	52.5	53
n_s	0.982		n_s	0.969	1.04
$-\alpha_s/10^{-4}$	3.4		$-\alpha_s/10^{-4}$	5.8	16.6

TABLE 2: Input and output parameters consistent with Eqs. (19) and (20) for shifted ($M_S = 5 \times 10^{17}$ GeV) or smooth FHI and $v_G = M_{\text{GUT}}$ with and without the mSUGRA contribution.

respectively which are obviously predictions of each FHI model – without the possibility of fulfilling Eq. (1) by some adjustment.

In the case of standard FHI with $N = 2$, we present the allowed by Eqs. (19) and (20) values of v_G versus κ (Fig. 5) and n_s versus κ (Fig. 6). Dashed [solid] lines indicate results obtained within SUSY [mSUGRA], i.e. by setting $V_{\text{HIS}} = V_{\text{HIT}} = 0$ [$V_{\text{HIS}} = V_{\text{HISm}}$ given by Eq. (10) and V_{HIT} given by Eq. (11) with $a_S=1$ TeV] in Eq. (6). We, thus, can easily identify the regimes where the several contributions to V_{HI} dominate. Namely, for $\kappa \gtrsim 0.01$, V_{HISm} dominates and drives n_s to values close to or larger than unity – see Fig. 6. On the other hand, for $5 \times 10^{-4} \lesssim \kappa \lesssim 0.01$, V_{HIc} becomes prominent. Finally, for $\kappa \lesssim 5 \times 10^{-3}$, V_{HIT} starts playing an important role and as v_G increases, V_{HISm} becomes again important. In Fig. 6 we also design with thin lines the region of Eq. (1). We deduce that there is a marginally allowed area with $0.983 \lesssim n_s \lesssim 0.99$. This occurs for

$$0.0015 \lesssim \kappa \lesssim 0.03 \quad \text{with} \quad 0.56 \lesssim v_G/(10^{16} \text{ GeV}) \lesssim 0.74.$$

in mSUGRA whereas in global SUSY we have $\kappa \gtrsim 0.0015$ and $0.56 \lesssim v_G/(10^{16} \text{ GeV}) \lesssim 0.7$. We realize that $v_G < M_{\text{GUT}}$ – note that $M_{\text{GUT}} = (2 \times 10^{16}/0.7)$ GeV where 2×10^{16} GeV is the mass acquired by the gauge bosons during the SUSY GUT breaking and 0.7 is the unified gauge coupling constant at the scale 2×10^{16} GeV.

In the cases of shifted and smooth FHI we confine ourselves to the values of the parameters which give $v_G = M_{\text{GUT}}$ and display the solutions consistent with Eqs. (19) and (20) in Table 2. We observe that the required κ in the case of shifted FHI is rather low and so, the inclusion of mSUGRA does not raise n_s , which remains within the range of Eq. (1). On the contrary, in the case of smooth FHI, n_s increases sharply within mSUGRA although the result in the absence of mSUGRA is slightly lower than this of shifted FHI. In the former case $|\alpha_s|$ is also considerably enhanced.

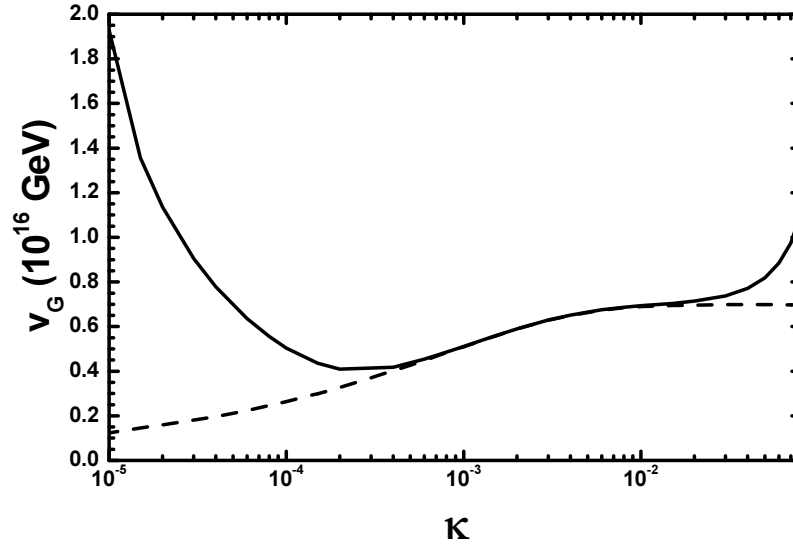


FIGURE 5: The allowed by Eqs. (19) and (20) values of v_G versus κ for standard FHI with $N = 2$ and $V_{\text{HIS}} = a_S = 0$ (dashed lines) or $V_{\text{HIS}} = V_{\text{HISm}}$ and $a_S = 1$ TeV (solid lines).

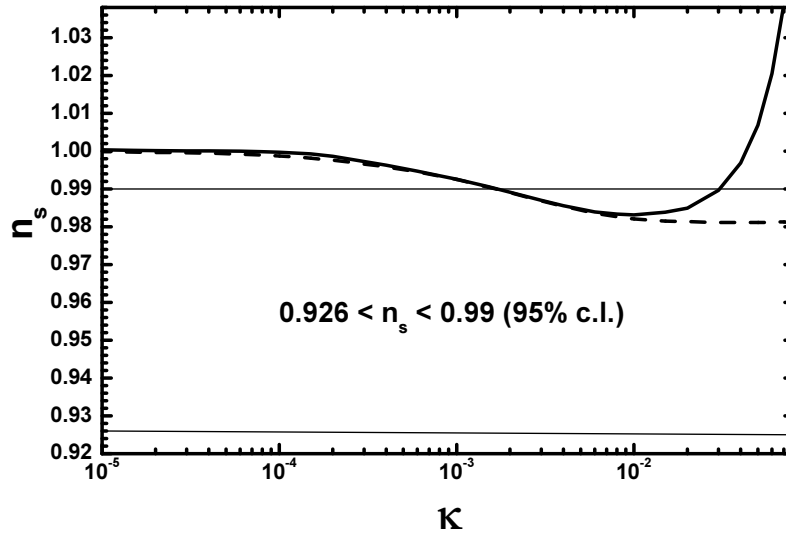


FIGURE 6: The allowed by Eqs. (19) and (20) values of n_s versus κ for standard FHI with $N = 2$ and $V_{\text{HIS}} = a_S = 0$ (dashed lines) or $V_{\text{HIS}} = V_{\text{HISm}}$ and $a_S = 1$ TeV (solid lines). The region of Eq. (1) is also limited by thin lines.

3 REDUCING n_s THROUGH QUASI-CANONICAL SUGRA

Sizeable variation of n_s in FHI can be achieved by considering a moderate deviation from mSUGRA, named [18] qSUGRA. The form of the relevant Kähler potential for σ is given by

$$K_q = \frac{\sigma^2}{2} \pm c_q \frac{\sigma^4}{4m_P^2} \quad (23)$$

with $c_q > 0$ a free parameter. Note that for $\sigma \ll m_P$ higher order terms in the expansion of Eq. (23) have no effect on the inflationary dynamics. Inserting Eq. (23) into Eq. (9), we obtain the corresponding contribution to V_{HI} ,

$$V_{\text{HISq}} \simeq V_{\text{HI0}} \left(\mp c_q \frac{\sigma^2}{2m_P^2} + c_{\text{qq}} \frac{\sigma^4}{8m_P^4} + \mathcal{O}\left(\frac{\sigma}{m_P}\right)^6 \right) \quad \text{with } c_{\text{qq}} = 1 - \frac{7}{2}c_q + \frac{5}{2}c_q^2. \quad (24)$$

The fitting of WMAP3 data by Λ CDM model obliges [16, 17, 20] us to consider the positive [minus] sign in Eq. (23) [Eq. (24)] (the opposite choice implies [18] a pronounced increase of n_s above unity). As a consequence V_{HI} acquires a rather interesting structure which is studied in Sec. 3.1. In Sec. 3.2 we specify the observational constraints which we impose to this scenario and in Sec. 3.3 we exhibit our numerical results.

3.1 THE STRUCTURE OF THE INFLATIONARY POTENTIAL

In the qSUGRA scenario the potential V_{HI} can be derived from Eq. (6) posing $V_{\text{HIS}} = V_{\text{HISq}}$ given by Eq. (24) with minus in the first term. Depending on the value of c_q , V_{HI} is a monotonic function of σ or develops a local minimum and maximum. The latter case leads to two possible complications: (i) The system gets trapped near the minimum of V_{HI} and, consequently, no FHI takes place and (ii) even if FHI of the so-called hilltop type [19] occurs with σ rolling from the region of the maximum down to smaller values, a mild tuning of the initial conditions is required [16] in order to obtain acceptable n_s 's.

It is, therefore, crucial to check if we can accomplish the aim above, avoiding [20, 21] the minimum-maximum structure of V_{HI} . In such a case the system can start its slow rolling from any point on the inflationary path without the danger of getting trapped. This can be achieved, if we require that V_{HI} is a monotonically increasing function of σ , i.e. $V'_{\text{HI}} > 0$ for any σ or, equivalently,

$$V'_{\text{HI}}(\bar{\sigma}_{\text{min}}) > 0 \quad \text{with} \quad V''_{\text{HI}}(\bar{\sigma}_{\text{min}}) = 0 \quad \text{and} \quad V'''_{\text{HI}}(\bar{\sigma}_{\text{min}}) > 0 \quad (25)$$

where $\bar{\sigma}_{\text{min}}$ is the value of σ at which the minimum of V'_{HI} lies. Employing the conditions of Eq. (25) we find approximately:

$$\bar{\sigma}_{\text{min}} \simeq \begin{cases} \sqrt{2c_q/3c_{\text{qq}}} m_P & \text{for standard and shifted FHI,} \\ \sqrt{2m_P/3} (\sqrt{5/c_{\text{qq}}} \mu_S M_S)^{1/4} & \text{for smooth FHI.} \end{cases} \quad (26)$$

Inserting Eq. (26) into Eq. (25), we find that V_{HI} remains monotonic for

$$c_q < c_q^{\text{max}} \text{ with } c_q^{\text{max}} = \begin{cases} 3\kappa\sqrt{c_{\text{qq}}\mathbb{N}}/4\sqrt{2}\pi & \text{for standard FHI,} \\ 3\kappa\sqrt{c_{\text{qq}}}/4\pi & \text{for shifted FHI,} \\ (8/3)(c_{\text{qq}}/5)^{3/4}\sqrt{\mu_S M_S}/m_{\text{P}} & \text{for smooth FHI.} \end{cases} \quad (27)$$

For $c_q > c_q^{\text{max}}$, V_{HI} reaches at the points σ_{min} [σ_{max}] a local minimum [maximum] which can be estimated as follows:

$$\sigma_{\text{min}} \simeq \sqrt{\frac{2c_q}{c_{\text{qq}}}}m_{\text{P}} \text{ and } \sigma_{\text{max}} \simeq \begin{cases} \kappa m_{\text{P}}\sqrt{\mathbb{N}}/2\sqrt{2c_q}\pi & \text{for standard FHI,} \\ \kappa m_{\text{P}}/2\sqrt{c_q}\pi & \text{for shifted FHI,} \\ \sqrt{2/3c_q}(\mu_S M_S m_{\text{P}})^{1/3} & \text{for smooth FHI.} \end{cases} \quad (28)$$

Even in this case, the system can always undergo FHI starting at $\sigma < \sigma_{\text{max}}$ since $V'_{\text{HI}}(\sigma_{\text{max}}) = 0$. However, the lower n_s we want to obtain, the closer we must set σ_* to σ_{max} . This signals [16] a substantial tuning in the initial conditions of FHI.

Employing the strategy outlined in Sec. (2.4) we can take a flavor for the expected n_s 's in the qSUGRA scenario, for any c_q :

$$n_s = \begin{cases} 1 - 2c_q(1 - 1/c_N) - 3c_{\text{qq}}\kappa^2\mathbb{N}c_N/4c_q\pi^2 & \text{for standard FHI,} \\ 1 - 2c_q(1 - 1/c_N) - 3c_{\text{qq}}\kappa^2c_N/4c_q\pi^2 & \text{for shifted FHI,} \\ 1 - 5/3N_{\text{HI}^*} + 2\tilde{c}_N - (2\tilde{c}_N N_{\text{HI}^*} + 7)c_q & \text{for smooth FHI,} \end{cases} \quad (29)$$

$$\text{with } c_N = 1 - \sqrt{1 + 4c_q N_{\text{HI}^*}} \text{ and } \tilde{c}_N = c_q (6\mu_S^2 M_S^2 N_{\text{HI}^*}/m_{\text{P}}^4)^{1/3}.$$

We can clearly appreciate the contribution of a positive c_q to the lowering of n_s .

3.2 OBSERVATIONAL CONSTRAINTS

As in the case of mSUGRA and under the same assumptions, the qSUGRA scenario needs to satisfy Eq. (19) and (20). However, due to the presence of the extra parameter c_q , a simultaneous fulfillment of Eq. (1) becomes [17, 16, 20] possible. In addition, we take into account, as optional constraint, Eq. (25) so as complications from the appearance of the minimum-maximum structure of V_{HI} are avoided.

It is worth mentioning that K_q in Eq. (23) generates a non-minimal kinetic term of σ thereby altering, in principle, the inflationary dynamics and the calculation of the inflationary observables. Indeed, the kinetic term of σ is

$$\frac{1}{2} \frac{\partial^2 K_q}{\partial S \partial S^*} \dot{\sigma}^2 \text{ with } \frac{\partial^2 K_q}{\partial S \partial S^*} = 1 \pm 2c_q \frac{\sigma^2}{m_{\text{P}}^2} \quad (30)$$

(the dot denotes derivation w.r.t the cosmic time). Assuming that the ‘friction’ term $3H\dot{\sigma}$ dominates over the other terms in the *equation of motion* (e.o.m) of σ , we can derive the slow roll parameters ϵ and η in Eq. (13) which carry an extra factor $(1 \pm 2c_q\sigma^2/m_{\text{P}}^2)^{-1}$, in the present case. The formulas in Eqs. (12) and (14) get modified also. In particular, a factor $(1 \pm 2c_q\sigma^2/m_{\text{P}}^2)$ must be included in the integrand in the *right-hand side* (r.h.s) of Eq. (12) and a factor $(1 \pm 2c_q\sigma^2/m_{\text{P}}^2)^{1/2}$ in the r.h.s of Eq. (14). However, these modifications are certainly numerically negligible since $\sigma \ll m_{\text{P}}$ and $c_q \ll 1$ (see Sec. 3.3).

3.3 NUMERICAL RESULTS

SHIFTED FHI				SMOOTH FHI			
n_s	0.926	0.958	0.976	n_s	0.926	0.958	0.99
$c_q/10^{-3}$	16.8	7.5	2	$c_q/10^{-3}$	11	8.3	5.45
$c_q^{\max}/10^{-3}$	1.7	1.87	2	$c_q^{\max}/10^{-3}$	9	9	9
$\sigma_*/10^{16}$ GeV	6.05	5.46	5.36	$\sigma_*/10^{16}$ GeV	23.1	24.5	26.5
$\kappa/10^{-3}$	7.8	8.45	9	$M_S/5 \times 10^{17}$ GeV	2.86	2.02	1.44
$M/10^{16}$ GeV	2.18	2.24	2.28	$\mu_S/10^{16}$ GeV	0.06	0.08	0.1
$1/\xi$	4.1	4.21	4.31	$\sigma_f/10^{16}$ GeV	13.4	13.4	13.4
N_{HI^*}	51.7	52	52	N_{HI^*}	52.2	52.4	52.6
$-\alpha_s/10^{-4}$	2.8	3.4	3.5	$-\alpha_s/10^{-3}$	0.56	0.8	1

TABLE 3: Input and output parameters consistent with Eqs. (19) and (20) for shifted ($M_S = 5 \times 10^{17}$ GeV) or smooth FHI, $v_G = M_{\text{GUT}}$ and selected n_s 's within the qSUGRA scenario.

Our strategy in the numerical investigation of the qSUGRA scenario is the one described in Sec. 2.6. In addition to the parameters manipulated there, here we have the parameter c_q which can be adjusted so as to achieve n_s in the range of Eq. (1). We check also the fulfillment of Eq. (25).

In the case of standard FHI with $N = 2$, we delineate the (lightly gray shaded) region allowed by Eqs. (1), (19) and (20) in the $\kappa - c_q$ (Fig. 7) and $\kappa - v_G$ (Fig. 8) plane. The conventions adopted for the various lines are also shown in the r.h.s of each graphs. In particular, the black solid [dashed] lines correspond to $n_s = 0.99$ [$n_s = 0.926$], whereas the gray solid lines have been obtained by fixing $n_s = 0.958$ – see Eq. (1). The dot-dashed lines correspond to $c_q = c_q^{\max}$ in Eq. (27) whereas the dotted line indicates the region in which Eq. (1) is fulfilled in the mSUGRA scenario. In the hatched region, Eq. (25) is also satisfied. We observe that the optimistic constraint of Eq. (25) can be met in a narrow but not unnaturally small fraction of the allowed area. Namely, for $n_s = 0.958$, we find

$$0.06 \lesssim \kappa \lesssim 0.15 \quad \text{with} \quad 0.47 \gtrsim v_G/(10^{16} \text{ GeV}) \gtrsim 0.37 \quad \text{and} \quad 0.013 \lesssim c_q \lesssim 0.03.$$

The lowest $n_s = 0.946$ can be achieved for $\kappa = 0.15$. Note that the v_G 's encountered here are lower than those found in the mSUGRA scenario (see Sec. 2.6).

In the cases of shifted and smooth FHI we confine ourselves to the values of the parameters which give $v_G = M_{\text{GUT}}$ and display in Table 3 their values which are also consistent with Eqs. (19) and (20) for selected n_s 's. In the case of shifted FHI, we observe that (i) it is not possible to obtain $n_s = 0.99$ since the mSUGRA result is lower (see Table 2) (ii) the lowest possible n_s compatible with the conditions of Eq. (25) is 0.976 and so, $n_s = 0.958$ is not consistent with Eq. (25). In the case of smooth FHI, we see that reduction of n_s consistently with Eq. (25) can be achieved for $n_s \gtrsim 0.951$ and so $n_s = 0.958$ can be obtained without complications.

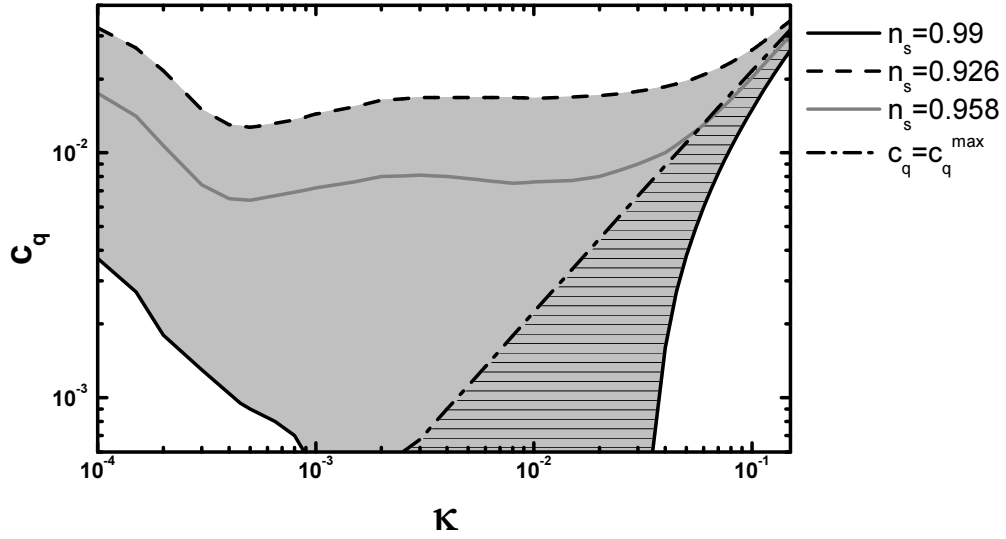


FIGURE 7: Allowed (lightly gray shaded) region in the $\kappa - c_q$ plane for standard FHI within the qSUGRA scenario. Ruled is the region where the inflationary potential remains monotonic. The conventions adopted for the various lines are also shown.

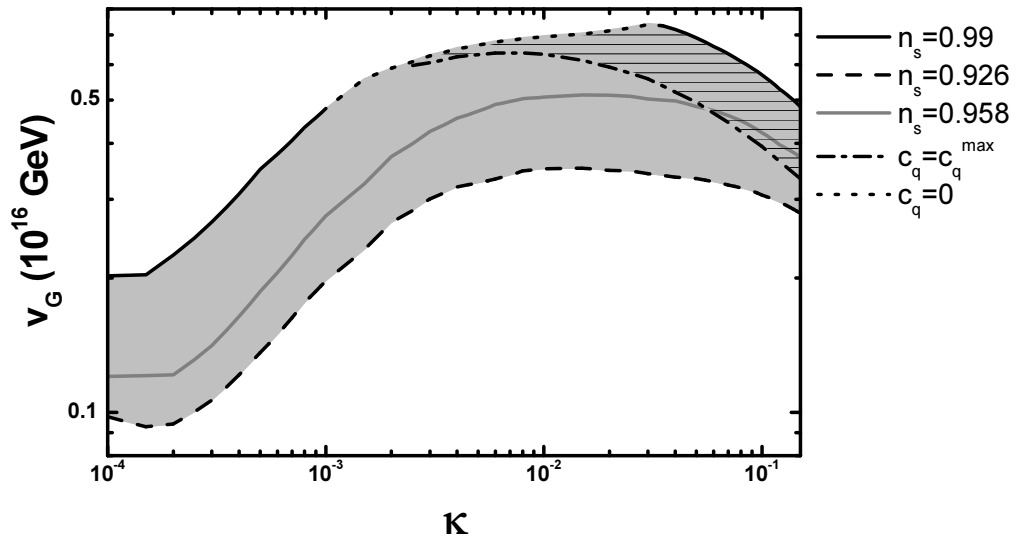


FIGURE 8: Allowed (lightly gray shaded) region in the $\kappa - v_G$ plane for standard FHI within the qSUGRA scenario. Ruled is the region where the inflationary potential remains monotonic. The conventions adopted for the various lines are also shown.

4 REDUCING n_s THROUGH A COMPLEMENTARY MI

Another, more drastic and radical, way to circumvent the n_s problem of FHI is the consideration of a double inflationary set-up. This proposition [22] is based on the observation that n_s within FHI models generally decreases [31] with N_{HI^*} – given by Eq. (12). This statement is induced by Eqs. (17) and (18) and can be confirmed by Fig. 9 where we draw n_s in standard FHI with $N = 1$ as a function of N_{HI^*} for several κ 's indicated in the graph. On the curves, Eq. (19) is satisfied. Therefore, we could constrain N_{HI^*} , fulfilling Eq. (1). Note that a constrained N_{HI^*} was also previously used in Ref. [34] to achieve a sufficient running of n_s .

The residual amount of e-foldings, required for the resolution of the horizon and flatness problems of the standard big-bang cosmology, can be generated during a subsequent stage of MI realized at a lower scale by a string modulus. We show that this scenario can satisfy a number of constraints with more or less natural values of the parameters. Such a construction is also beneficial for MI, since the perturbations of the inflaton field in this model are not sufficiently large to account for the observations, due to the low inflationary energy scale.

Let us also mention that MI naturally assures a low reheat temperature. As a consequence, the gravitino constraint [29] on the reheat temperature of FHI and the potential topological defect problem of standard FHI [30] can be significantly relaxed or completely evaded. On the other hand, for the same reason baryogenesis is made more difficult, since any preexisting baryon asymmetry is diluted by the entropy production during the modulus decay. However, it is not impossible to achieve adequate baryogenesis in the scheme of cold electroweak baryogenesis [35] or in the context of (large) extra dimensions [36].

The main features of MI are sketched in Sec. 4.1. The parameter space of the present scenario is restricted in Sec. 4.3 taking into account a number of observational requirements which are exhibited in Sec. 4.2

4.1 THE BASICS OF MI

Fields having (mostly Planck scale) suppressed couplings to the SM degrees of freedom and weak scale (non-SUSY) mass are called collectively moduli. After the gravity mediated soft SUSY breaking, their potential can take the form (see the appendix A in Ref. [37]):

$$V_{\text{MI}} = (m_{3/2} m_{\text{P}})^2 \mathcal{V} \left(\frac{s}{m_{\text{P}}} \right) \quad (31)$$

where \mathcal{V} is a function with dimensionless coefficients of order unity and s is the canonically normalized, axionic or radial component of a string modulus. MI is usually supposed [23] to take place near a maximum of V_{MI} , which can be expanded as follows:

$$V_{\text{MI}} \simeq V_{\text{MI0}} - \frac{1}{2} m_s^2 s^2 + \dots, \quad (32)$$

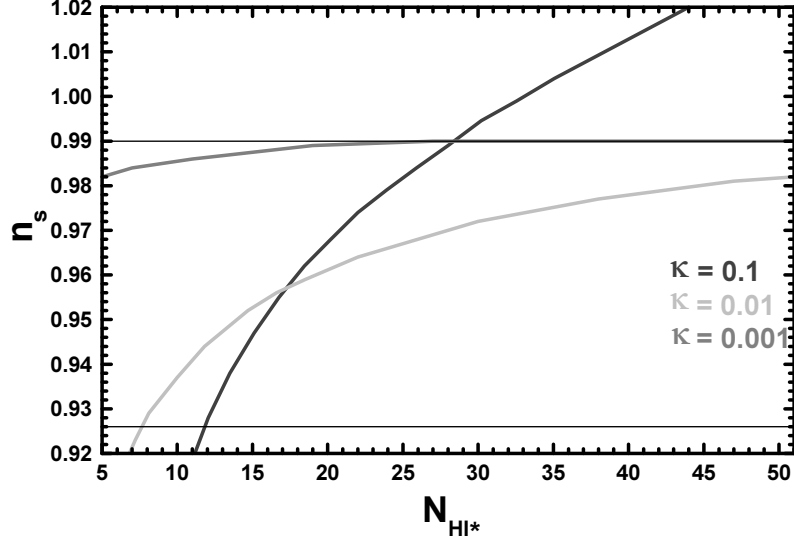


FIGURE 9: The spectral index n_s in standard FHI as a function of N_{HI^*} for several κ 's indicated in the graph. On the curves, Eq. (19) is satisfied.

where the ellipsis denotes terms which are expected to stabilize V_{MI} at $s \sim m_{\text{P}}$. Comparing Eqs. (31) and (32), we conclude that

$$V_{\text{MI}0} = v_s (m_{3/2} m_{\text{P}})^2 \quad \text{and} \quad m_s \sim m_{3/2}, \quad (33)$$

where $m_{3/2} \sim 1$ TeV is the gravitino mass and the coefficient v_s is of order unity, yielding $V_{\text{MI}0}^{1/4} \simeq 3 \times 10^{10}$ GeV. However, if s has just Planck scale suppressed interactions to light degrees of freedom, NS constraint forces [43] us to use (see Sec. 4.2) much larger values for m_s and $m_{3/2}$. In Fig. 10, we present a typical example of the (dimensionless) potential $V_{\text{MI}}/(m_{3/2} m_{\text{P}})^2$ versus s/m_{P} , where the constant quantity $c_{\text{MI}0} \simeq 0.7$ has been subtracted so that $V_{\text{MI}}/(m_{3/2} m_{\text{P}})^2$ vanishes at its absolute minimum (the subscript 0 of $V_{\text{MI}0}$ and $c_{\text{MI}0}$ is not referred to present-day values).

Solving the e.o.m of the field s (the dot denotes derivation w.r.t the cosmic time),

$$\ddot{s} + 3Hs + d^2V/ds^2 = 0, \quad (34)$$

for $H = H_s \simeq \sqrt{V_{\text{MI}0}}/\sqrt{3}m_{\text{P}}$ and $V = V_{\text{MI}} \Rightarrow d^2V/ds^2 \simeq -m_s^2$, we can extract [27] its evolution during MI:

$$s = s_{\text{MI}} e^{F_s \Delta N_{\text{MI}}} \quad \text{with} \quad F_s \equiv \sqrt{\frac{9}{4} + \left(\frac{m_s}{H_s}\right)^2} - \frac{3}{2}. \quad (35)$$

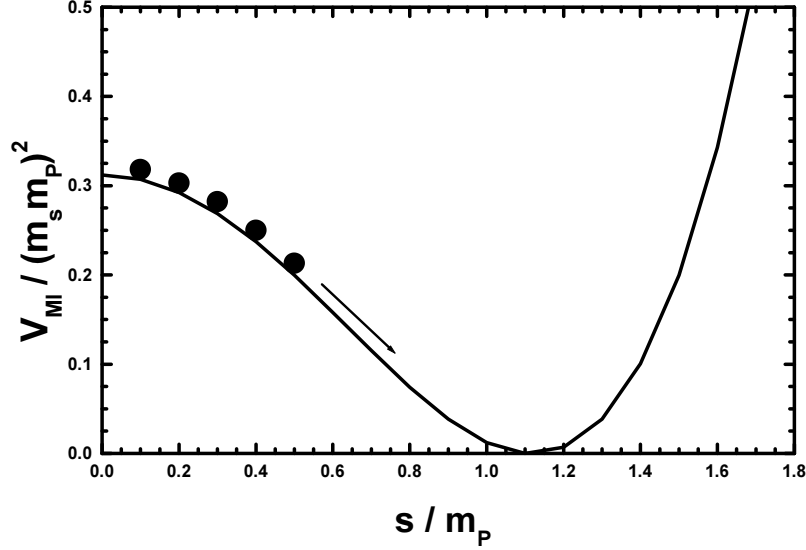


FIGURE 10: The (dimensionless) potential $V_{\text{MI}}/(m_{3/2}m_{\text{P}})^2 = 1 - 0.5(s/m_{\text{P}})^2 + 0.2(s/m_{\text{P}})^4 - c_{\text{MI}0}$ versus s/m_{P} . The inflationary trajectory is also depicted by black points.

Here, s_{MI} is the value of s at the onset of MI and ΔN_{MI} is the number of the e-foldings obtained from $s = s_{\text{MI}}$ until a given s . For natural MI we need:

$$0.5 \leq v_s \leq 10 \Rightarrow 2.45 \geq m_s/H_s \geq 0.55 \Rightarrow 1.37 \geq F_s \geq 0.097. \quad (36)$$

where the lower bound on v_s comes from the obvious requirement $V_{\text{MI}} > 0$.

In this model, inflation can be not only of the slow-roll but also of the fast-roll [27] type. This is, because there is a range of parameters where, although the ϵ -criterion for MI, $\epsilon_s < 1$, is fulfilled, the η -criterion, $\eta_s < 1$, is violated giving rise to fast-roll inflation. Indeed, using its most general form [4], ϵ_s reads:

$$\epsilon_s = -\frac{\dot{H}_{\text{MI}}}{H_{\text{MI}}^2} = F_s^2 \frac{s^2}{2m_{\text{P}}^2}, \quad (37)$$

where the former expression can be derived inserting Eq. (35) into Eq. (34) with $H = H_{\text{MI}} = \sqrt{V_{\text{MI}}}/\sqrt{3}m_{\text{P}}$. Numerically we find:

$$0.005 \leq \epsilon_s \leq 0.94 \text{ for } 0.55 \leq m_s/H_s \leq 2.45 \text{ and } s/m_{\text{P}} = 1. \quad (38)$$

Therefore, we can obtain accelerated expansion (i.e. inflation) with $H_s \simeq \text{cst}$. Note, though, that near the upper bound on m_s/H_s , ϵ_s gets too close to unity at $s = m_{\text{P}}$ and thus, H_s does not remain constant as s approaches m_{P} . Therefore, our results at large values

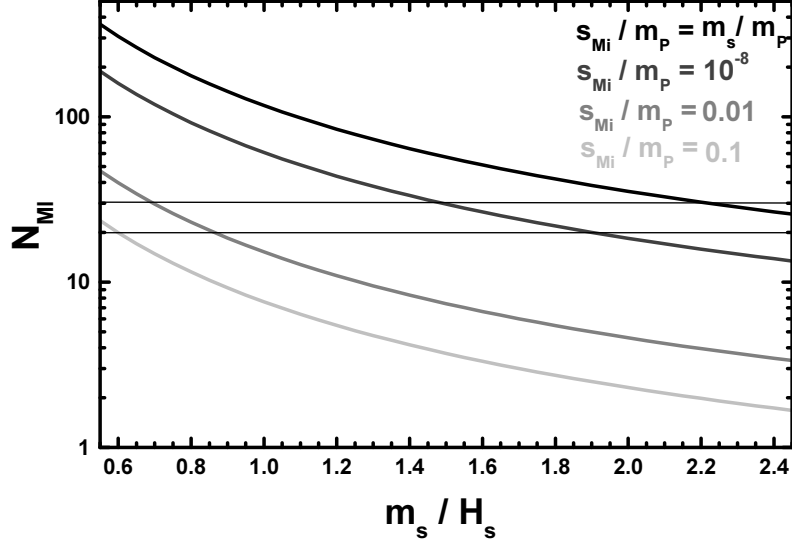


FIGURE 11: The number of e -foldings N_{MI} obtained during MI as a function of m_s/H_s for $s_{\text{Mf}}/m_{\text{P}} = 1$ and several s_i/m_{P} 's indicated in the graph. The required values of N_{MI} for a successful complementary MI is approximately limited by two thin line.

of m_s/H_s should be considered only as indicative. On the other hand, η_s can be larger or lower than 1, since:

$$|\eta_s| = m_{\text{P}}^2 \frac{|d^2 V_{\text{MI}}/ds^2|}{V_{\text{MI}}} = \frac{m_s^2}{3H_s^2} \simeq \frac{1}{v_s} \quad (39)$$

where the last equality holds for $m_s = m_{3/2}$. Therefore, the condition which discriminates the slow-roll from the fast-roll MI is:

$$\begin{cases} m_s/H_s < \sqrt{3} & \text{or } v_s > 1 & \text{for slow-roll MI,} \\ m_s/H_s > \sqrt{3} & \text{or } v_s < 1 & \text{for fast-roll MI.} \end{cases} \quad (40)$$

The total number of e -foldings during MI can be found from Eq. (35). Namely,

$$N_{\text{MI}} = \frac{1}{F_s} \ln \frac{s_{\text{Mf}}}{s_{\text{Mi}}} \simeq \frac{1}{F_s} \ln \frac{m_{\text{P}}}{s_{\text{Mi}}}. \quad (41)$$

In our computation we take for the value of s at the end of MI $s_{\text{Mf}} = m_{\text{P}}$, since the condition $\epsilon_s = 1$ gives $s_{\text{Mf}}/m_{\text{P}} = \sqrt{2}/F_s > 1$, for the ranges of Eq. (36). This result is found because the (unspecified) terms in the ellipsis in the r.h.s of Eq. (32) starts playing an important role for $s \sim m_{\text{P}}$ and it is obviously unacceptable.

In Fig. 11, we depict N_{MI} versus m_s/H_s for $s_{\text{Mf}} = m_{\text{P}}$ and several $s_{\text{Mi}}/m_{\text{P}}$'s indicated in the graph. We observe that N_{MI} is very sensitive to the variations of m_s/H_s . Also, taking into account that $20 \lesssim N_{\text{MI}} \lesssim 30$ (limited in Fig. 11 by two thin lines) is needed so that

MI plays successfully the role of complementary inflation (see Sec. 4.3), we can deduce the following:

- As s_{Mi} decreases, the required m_s/H_s for obtaining $N_{\text{MI}} \sim 30$ increases. To this end, for $s_{\text{Mi}}/m_{\text{P}} \lesssim 10^{-8}$ [$s_{\text{Mi}}/m_{\text{P}} \gtrsim 10^{-8}$], we need fast-roll [slow-roll] MI.
- For $s_{\text{Mi}}/m_{\text{P}} \gtrsim 0.1$, it is not possible to obtain $N_{\text{MI}} \sim 30$ and so, MI can not play successfully the role of complementary inflation.

4.2 OBSERVATIONAL CONSTRAINTS

In addition to Eqs. (1) and (19) – on the assumption that the inflaton perturbation generates exclusively the curvature perturbation – the cosmological scenario under consideration needs to satisfy a number of other constraints too. These can be outlined as follows:

- (i) The horizon and flatness problems of SBB can be successfully resolved provided that the scale k_* suffered a certain total number of e-foldings N_{tot} . In the present set-up, N_{tot} consists of two contributions:

$$N_{\text{tot}} = N_{\text{HI}^*} + N_{\text{MI}}. \quad (42)$$

Employing the conventions and the strategy we applied in the derivation of Eq. (21), we can find [38] the number of e-foldings N_k between horizon crossing of the observationally relevant mode k and the end of FHI as follows:

$$\begin{aligned} \frac{k}{H_0 R_0} &= \frac{H_k R_k}{H_0 R_0} \\ &= \frac{H_k}{H_0} \frac{R_k}{R_{\text{Hf}}} \frac{R_{\text{Mi}}}{R_{\text{Mi}}} \frac{R_{\text{Mf}}}{R_{\text{Mf}}} \frac{R_{\text{Mrh}}}{R_{\text{Mrh}}} \frac{R_{\text{eq}}}{R_{\text{eq}}} \frac{R_0}{R_0} \\ &= \sqrt{\frac{V_{\text{HI0}}}{\rho_{\text{c0}}}} e^{-N_k} \left(\frac{V_{\text{HI0}}}{V_{\text{MI0}}} \right)^{-1/3} e^{-N_{\text{MI}}} \left(\frac{V_{\text{MI0}}}{\rho_{\text{Mrh}}} \right)^{-1/3} \left(\frac{\rho_{\text{Mrh}}}{\rho_{\text{eq}}} \right)^{-1/4} \left(\frac{\rho_{\text{eq}}}{\rho_{\text{m0}}} \right)^{-1/3} \\ &\Rightarrow N_k + N_{\text{MI}} \simeq \ln \frac{H_0 R_0}{k} + 24.72 + \frac{2}{3} \ln \frac{V_{\text{HI0}}^{1/4}}{1 \text{ GeV}} + \frac{1}{3} \ln \frac{T_{\text{Mrh}}}{1 \text{ GeV}}. \end{aligned} \quad (43)$$

Here, we have assumed that the reheat temperature after FHI, T_{Hrh} is lower than $V_{\text{MI0}}^{1/4}$ (as in the majority of these models [5]) and, thus, we obtain just MD during the inter-inflationary era. Also, the subscripts Mi, Mf, Mrh denote values at the onset of MI, at the end of MI and at the end of the reheating after the completion of the MI. Inserting into Eq. (43) $H_0 = 2.37 \times 10^{-4}/\text{Mpc}$ and $k/R_0 = 0.002/\text{Mpc}$ and taking into account Eq. (42), we can easily derive the required N_{tot} at k_* :

$$N_{\text{HI}^*} + N_{\text{MI}} \simeq 22.6 + \frac{2}{3} \ln \frac{V_{\text{HI0}}^{1/4}}{1 \text{ GeV}} + \frac{1}{3} \ln \frac{T_{\text{Mrh}}}{1 \text{ GeV}}. \quad (44)$$

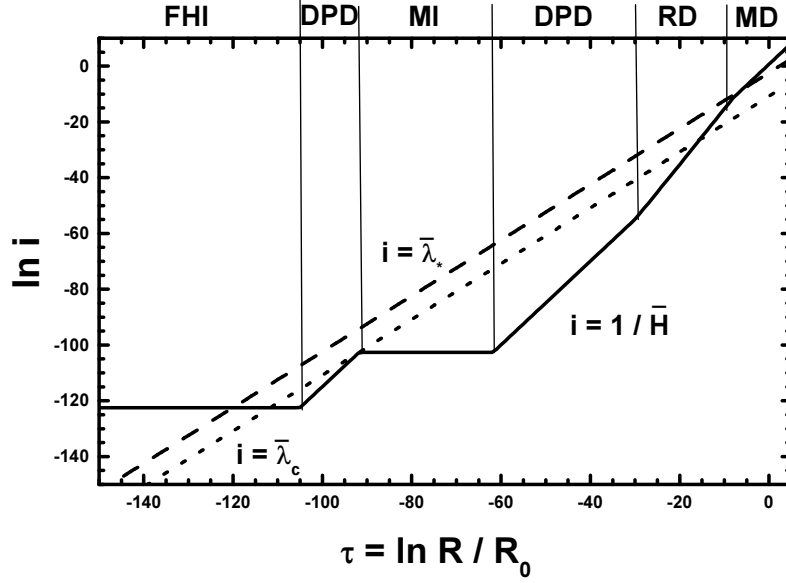


FIGURE 12: The evolution of the quantities $1/\bar{H} = H_0/H$ (solid line), $\bar{\lambda}_* = \lambda_*/R_0$ (dashed line) and $\bar{\lambda}_c = \lambda_c/R_0$ (dotted line) as a function of τ for $V_{\text{HI0}}^{1/4} = 10^{15}$ GeV, $N_{\text{HI}*} \simeq 15$, $V_{\text{MIO}}^{1/4} = 5 \times 10^{10}$ GeV, $N_{\text{MI}} \simeq 30$ and $T_{\text{Mrh}} = 1$ GeV. The various eras of the cosmological evolution are also shown.

The cosmological evolution followed in the derivation of Eq. (43) is illustrated in Fig. 12 where we design the (dimensionless) physical length $\bar{\lambda}_* = \lambda_*/R_0$ (dashed line) corresponding to k_* and the (dimensionless) particle horizon $\bar{R}_H = 1/\bar{H} = H_0/H$ (solid line) as a function of $\tau = \ln R/R_0$. In this plot we take $V_{\text{HI0}}^{1/4} = 10^{15}$ GeV, $N_{\text{HI}*} \simeq 15$, $V_{\text{MIO}}^{1/4} = 5 \times 10^{10}$ GeV, $N_{\text{MI}} \simeq 30$, and $T_{\text{Mrh}} = 1$ GeV. We take also $\bar{R}_H = H_0/H_s$ for MI. The various eras of the cosmological evolution are also clearly shown (compare with Fig. 4).

(ii) Taking into account that the range of the cosmological scales which can be probed by the CMB anisotropy is [2] $10^{-4}/\text{Mpc} \leq k \leq 0.1/\text{Mpc}$ (length scales of the order of 10 Mpc are starting to feel nonlinear effects and it is, thus, difficult to constrain [39] primordial density fluctuations on smaller scales) we have to assure that all the cosmological scales:

- Leave the horizon during FHI. This entails:

$$N_{\text{HI}*} \gtrsim N_k(k = 0.002/\text{Mpc}) - N_k(k = 0.1/\text{Mpc}) = 3.9 \quad (45)$$

which is the number of e-foldings elapsed between the horizon crossing of the pivot scale k_* and the scale $0.1/\text{Mpc}$ during FHI.

- Do not re-enter the horizon before the onset of MI (this would be possible since the scale factor increases during the inter-inflationary MD era [38]). This requires $N_{\text{HI}^*} \gtrsim N_{\text{HIc}}$, where N_{HIc} is the number of e-foldings elapsed between the horizon crossing of a wavelength k_c (which corresponds to the dimensionless length scale $\bar{\lambda}_c = \lambda_c/R_0$ depicted by a dotted line in Fig. 12) and the end of FHI. More specifically, k_c is to be such that:

$$1 = \frac{k_c}{H_{\text{MI}} R_{\text{MI}}} = \frac{H_c R_c}{H_s R_{\text{Hf}}} \frac{R_{\text{Hf}}}{R_{\text{MI}}} = e^{-N_{\text{HIc}}} \left(\frac{V_{\text{HI0}}}{V_{\text{MI0}}} \right)^{1/6} \Rightarrow N_{\text{HIc}} = \frac{1}{6} \ln \frac{V_{\text{HI0}}}{V_{\text{MI0}}}. \quad (46)$$

Both these requirements can be met if we demand [38]

$$N_{\text{HI}^*} \gtrsim N_{\text{HI}^*}^{\text{min}} \simeq 3.9 + \frac{1}{6} \ln \frac{V_{\text{HI0}}}{V_{\text{MI0}}}. \quad (47)$$

We expect $N_{\text{HI}^*}^{\text{min}} \sim 10$ since $(V_{\text{HI0}}/V_{\text{MI0}})^{1/4} \sim 10^{14}/10^{10} \sim 10^4$ and $\ln(10^{16})/6 \sim 6$.

(iii) As it is well known [31, 34], in the FHI models, $|\alpha_s|$ increases as N_{HI^*} decreases. Therefore, limiting ourselves to $|\alpha_s|$'s consistent with the assumptions of the power-law Λ CDM model, we obtain a lower bound on N_{HI^*} . Since, within the cosmological models with running spectral index, $|\alpha_s|$'s of order 0.01 are encountered [11], we impose the following upper bound on $|\alpha_s|$:

$$|\alpha_s| \ll 0.01. \quad (48)$$

(iv) Using the bounds of Eq. (36), we can find the corresponding bounds on N_{MI} . Namely,

$$0.73 \ln \frac{m_{\text{P}}}{s_{\text{MI}}} \leq N_{\text{MI}} \leq 10.2 \ln \frac{m_{\text{P}}}{s_{\text{MI}}}. \quad (49)$$

The relevant for our analysis (see Sec. 4.3) is the lower bound on N_{MI} which is $N_{\text{MI}}^{\text{min}} \sim 3$ for $s_{\text{MI}}/m_{\text{P}} = 0.01$ or $N_{\text{MI}}^{\text{min}} \sim 25$ for $s_{\text{MI}} \sim H_s$ and $m_s = m_{3/2} = 1$ TeV.

(v) Restrictions on the parameters can be also imposed from the evolution of the field s before MI. Depending whether s acquires or not effective mass [25, 26] during FHI and the inter-inflationary era, we can distinguish the cases:

- If s does not acquire mass (e.g. if s represents the axionic component of a string modulus or if a specific form for the Kähler potential of s has been adopted), we assume that FHI lasts long enough so that the value of s is completely randomized [40] as a consequence of its quantum fluctuations from FHI. We further require that all the values of s belong to the randomization region, which dictates [40] that

$$V_{\text{MI0}} \leq H_{\text{HI0}}^4 \text{ where } H_{\text{HI0}}^2 = V_{\text{HI0}}/3m_{\text{P}}^2. \quad (50)$$

Under these circumstances, all the initial values s_{Mi} of s from zero to m_{P} are equally probable – e.g. the probability to obtain $s_{\text{Mi}}/m_{\text{P}} \leq 0.01$ is $1/100$. Furthermore, the field s remains practically frozen during the inter-inflationary period since the Hubble parameter is larger than its mass.

- If s acquires effective mass of the order of H_{HI0} (as is [25, 26] generally expected) via the SUGRA scalar potential in Eq. (9), the field s can decrease to small values until the onset of MI. In our analysis we assume that:
 - The inflaton S has minimal Kähler potential $K_{\text{m}} = |S|^2$ and therefore, induces [25] an effective mass to s during FHI, $m_{s|\text{HI}} = \sqrt{3}H_{\text{HI0}}$.
 - The modulus s is decoupled from the visible sector superfields both in Kähler potential and superpotential and has canonical Kähler potential, $K_s = s^2/2$. In such a simplified case, the value s_{min} at which the SUGRA potential has a minimum is [28] $s_{\text{min}} = 0$.

Following Refs. [34, 41], the evolution of s can be found by solving its e.o.m. More explicitly, inserting into Eq. (34),

- $H = H_{\text{HI0}}$ and $V = (m_{s|\text{HI}})^2 s^2/2$ with $(m_{s|\text{HI}})^2 = 3H_{\text{HI0}}^2$, we can derive the value of s at the end of FHI:

$$s_{\text{Hf}} = s_{\text{Hi}} e^{-3N_{\text{HI}}/2} \left(\cos \frac{\sqrt{3}}{2} N_{\text{HI}} + \sin \frac{\sqrt{3}}{2} N_{\text{HI}} \right), \quad (51)$$

where $s_{\text{Hi}} \sim m_{\text{P}}$ is the value of s at the onset of FHI and N_{HI} is the total number of e-foldings obtained during FHI. We have also imposed the initial conditions, $s(N=0) = s_{\text{Hi}}$ and $ds(N=0)/dN = 0$.

- $H = H_{\text{HI0}} e^{-3\bar{N}/2}$ with $\bar{N} = \ln(R/R_{\text{Hf}})$ and $V = (m_{s|\text{MD}})^2 s^2/2$ with $(m_{s|\text{MD}})^2 = 3H^2/2$, we can derive the value of s at the beginig of MI:

$$s_{\text{Mi}} = s_{\text{Hf}} \left(\frac{V_{\text{MI0}}}{V_{\text{HI0}}} \right)^{1/4} \left(\cos \frac{\sqrt{15}}{12} \ln \frac{V_{\text{HI0}}}{V_{\text{MI0}}} + \sqrt{\frac{3}{5}} \sin \frac{\sqrt{15}}{12} \ln \frac{V_{\text{HI0}}}{V_{\text{MI0}}} \right), \quad (52)$$

where we have taken into account that during the inter-inflationary MD epoch $R \propto \rho^{-1/3}$ and imposed the initial conditions, $s(\bar{N}=0) = s_{\text{Hf}}$ and $ds(\bar{N}=0)/d\bar{N} = 0$.

In conclusion, combining Eqs. (51) and (52) we find

$$s_{\text{Mi}} \simeq m_{\text{P}} \left(\frac{V_{\text{MI0}}}{V_{\text{HI0}}} \right)^{1/4} e^{-3N_{\text{HI}}/2}. \quad (53)$$

(vi) In our analysis we have to ensure that the homogeneity of our present universe is not jeopardized by the quantum fluctuations of s during FHI which enter the horizon of MI, $\delta s|_{\text{HMI}}$ and during MI $\delta s|_{\text{MI}}$. Therefore, we have to dictate

$$s_{\text{MI}} \gg \delta s|_{\text{HMI}} \quad \text{and} \quad s_{\text{MI}} \gg \delta s|_{\text{MI}} \simeq H_s/2\pi. \quad (54)$$

In order to estimate $\delta s|_{\text{HMI}}$, we find it convenient to single out the cases:

- If s does not acquire mass before MI, $\delta s|_{\text{HMI}}$ remains frozen during FHI and the inter-inflationary era. Consequently, we get

$$\delta s|_{\text{HMI}} \simeq H_{\text{HI0}}/2\pi. \quad (55)$$

Obviously the first inequality in Eq. (54) is much more restrictive than the second one since $H_{\text{HI0}} \sim 10^{10}$ GeV whereas $H_s \sim m_s$.

- If s acquires mass before MI, we find [34, 41]:

$$\delta s|_{\text{HMI}} \simeq \frac{H_{\text{HI0}}}{2\pi} \left(\frac{H_{\text{HI0}}}{m_s|_{\text{HI}}} \right)^{1/2} e^{-3N_{\text{HIC}}/2} \left(\frac{V_{\text{MI0}}}{V_{\text{HI0}}} \right)^{1/4} = \frac{H_s}{3^{1/4} 2\pi}, \quad (56)$$

where Eq. (46) has been applied. As a consequence, the second inequality in Eq. (54) is roughly more restrictive than the first one and leads via Eq. (53) to the restriction:

$$N_{\text{HI}} \leq N_{\text{HI}}^{\text{max}} \quad \text{with} \quad N_{\text{HI}}^{\text{max}} = -\frac{2}{3} \ln \frac{(V_{\text{HI0}} V_{\text{MI0}})^{1/4}}{2\sqrt{3}\pi m_{\text{P}}^2}. \quad (57)$$

Given that $V_{\text{HI0}}^{1/4} \sim 10^{14}$ GeV and $V_{\text{MI0}}^{1/4} \sim 10^{10}$ GeV, we expect $N_{\text{HI}}^{\text{max}} \sim (15 - 18)$. This result signalizes an ugly tuning since it would be more reasonable FHI has a long duration due to the flatness of V_{HI} . This tuning could be evaded in a more elaborated set-up which would assure that $s_{\text{min}} \neq 0$, due to the fact that s would not be completely decoupled – as in Refs. [34, 41].

(vii) If s decays exclusively through gravitational couplings, its decay width Γ_s and, consequently, T_{Mrh} are highly suppressed [42, 43]. In particular,

$$\Gamma_s = \frac{1}{8\pi} \frac{m_s^3}{m_{\text{P}}^2} \quad \text{and} \quad [45] \quad T_{\text{Mrh}} = \left(\frac{72}{5g_{\rho^*}(T_{\text{Mrh}})} \right)^{1/4} \sqrt{\Gamma_s m_{\text{P}}/\pi} \quad (58)$$

with $g_{\rho^*}(T_{\text{Mrh}}) \simeq 76$. For $m_s \sim 1$ TeV, we obtain $T_{\text{Mrh}} \simeq 10$ keV which spoils the success of NS within SBB, since RD era must have already begun before NS takes place at $T_{\text{NS}} \simeq 1$ MeV. This is [42] the well known moduli problem. The easiest (although somehow tuned) resolution to this problem is [42, 43] the imposition of the condition (for alternative proposals see Refs. [28, 43]):

$$m_s \geq 100 \text{ TeV} \quad \text{which ensures} \quad T_{\text{Mrh}} \geq T_{\text{NS}}. \quad (59)$$

To avoid the so-called [44] moduli-induced gravitino problem too, $m_{3/2}$ is to increase accordingly.

4.3 NUMERICAL RESULTS

In addition to the parameters mentioned in Sec. 2.6, our numerical analysis depends on the parameters:

$$m_{3/2}, m_s, m_s/H_s, s_{\text{Mi}}.$$

We take throughout $m_{3/2} = m_s = 100$ TeV which results to $T_{\text{Mrh}} = 1.5$ MeV through Eq. (58) and assures the satisfaction of the NS constraint with almost the lowest possible m_s . Since T_{Mrh} appears in Eq. (44) through its logarithm, its variation has a minor influence on the value of N_{tot} and, therefore, on our results. On the contrary, the hierarchy between $m_{3/2}$ and m_s plays an important role, because N_{MI} depends crucially only on F_s – see Eq. (35) – which in turn depends on the ratio m_s/H_s with $H_s \sim m_{3/2}$. As justified in the point (vii) we consider the choice $m_s \sim m_{3/2}$ as the most natural. It is worth mentioning, finally, that the chosen value of m_s (and $m_{3/2}$) has a key impact on the allowed parameter space of this scenario, when s does not acquire mass before MI. This is, because m_s is explicitly related to V_{MI0} – see Eq. (33) – which, in turn, is involved in Eq. (50) and constrains strongly H_{HI0} – see point (i) below.

As in Sec. 2.6, we use as input parameters κ (for standard and shifted FHI with fixed $M_S = 5 \times 10^{17}$ GeV) or M_S (for smooth FHI) and σ_* . Employing Eqs. (15) and (19), we can extract n_s and v_G respectively. For every chosen κ or M_S , we then restrict σ_* so as to achieve n_s in the range of Eq. (1) and take the output values of N_{HI^*} (contrary to our strategy in Sec. 2.6 in which N_{HI^*} given by Eq. (20) is treated as a constraint and n_s is an output parameter). Finally, for every given s_{Mi} , we find from Eq. (44) the required N_{MI} and the corresponding v_s or m_s/H_s from Eq. (41). Replacing F_s from Eqs. (35) in Eq. (41) and solving w.r.t m_s/H_s , we find:

$$\frac{m_s}{H_s} = \sqrt{\frac{1}{N_{\text{MI}}} \ln \frac{m_{\text{P}}}{s_{\text{Mi}}} \left(\frac{1}{N_{\text{MI}}} \ln \frac{m_{\text{P}}}{s_{\text{Mi}}} + 3 \right)} \quad (60)$$

As regards the value of s_{Mi} we distinguish, once again, the cases:

(i) If s remains massless before MI, we choose $s_{\text{Mi}}/m_{\text{P}} = 0.01$. This value is close enough to m_{P} to have a non-negligible probability to be achieved by the randomization of s during FHI (see point (v) in Sec. 4.2). At the same time, it is adequately smaller than m_{P} to guarantee good accuracy of Eqs. (35) and (41) near the interesting solutions and justify the fact that we neglect the uncertainty from the terms in the ellipsis in Eq. (32) – since we can obtain $N_{\text{MI}} \sim 30$ with low m_s/H_s 's which assures low ϵ_s 's as we emphasize in Eq. (38). Moreover, larger s_{Mi} 's lead to smaller parameter space for interesting solutions (with n_s near its central value).

Our results are presented in Figs. 13 – 16 for standard FHI (with $N = 2$) and in Table 4 for shifted and smooth FHI. Let us discuss each case separately:

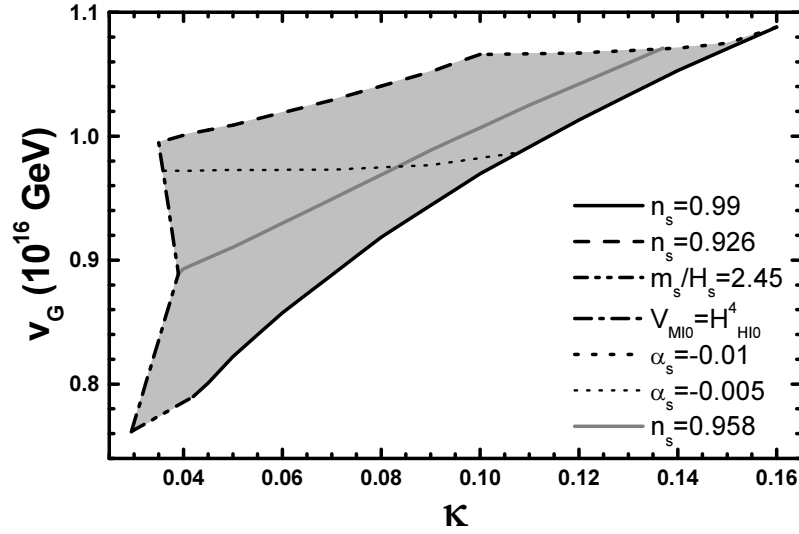


FIGURE 13: Allowed (lightly gray shaded) region in the $\kappa - v_G$ plane for standard FHI followed by MI realized by a field which remains massless before MI. The conventions adopted for the various lines are also shown.

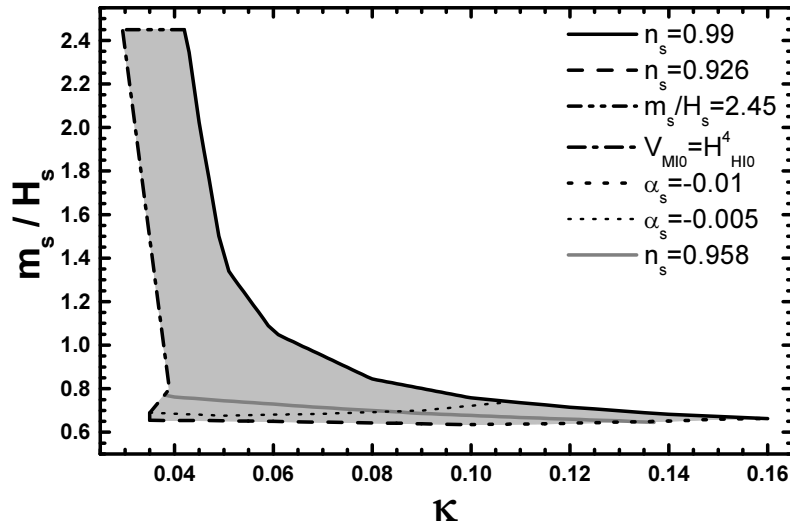


FIGURE 14: Allowed (lightly gray shaded) regions in the $\kappa - m_s/H_s$ plane for standard FHI followed by MI realized by a field which remains massless before MI. The conventions adopted for the various lines are also shown.

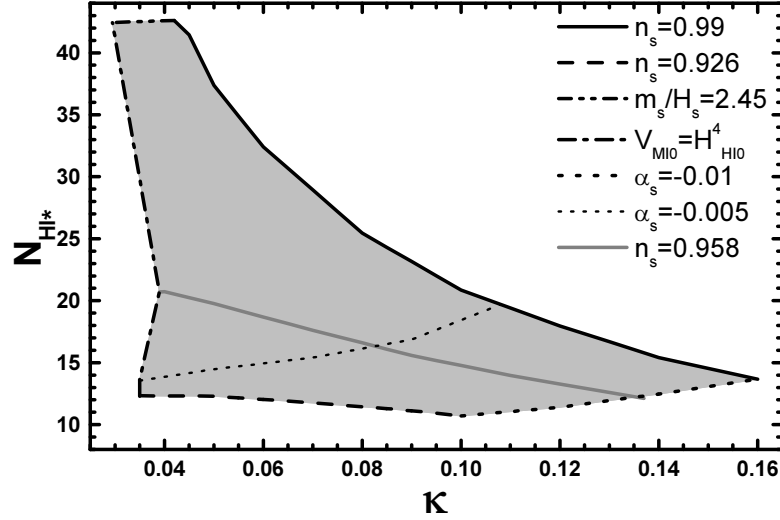


FIGURE 15: Allowed (lightly gray shaded) region in the $\kappa - N_{\text{HI}^*}$ plane for standard FHI followed by MI realized by a field which remains massless before MI. The conventions adopted for the various lines are also shown.

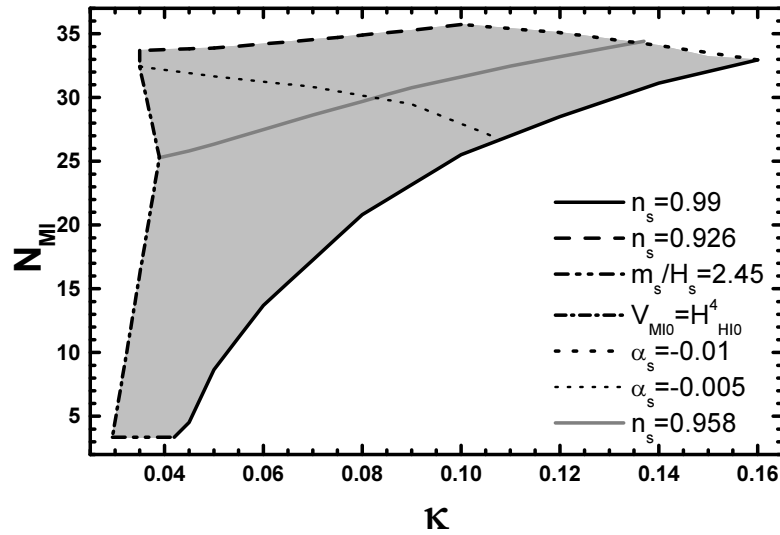


FIGURE 16: Allowed (lightly gray shaded) region in the $\kappa - N_{\text{MI}}$ plane for standard FHI followed by MI realized by a field which remains massless before MI. The conventions adopted for the various lines are also shown.

- **Standard FHI.** We present the regions allowed by Eqs. (1), (19), (44), (47) – (50), (54) and (59) in the $\kappa - v_G$ (Fig. 13), $\kappa - m_s/H_s$ (Fig. 14), $\kappa - N_{\text{HI}^*}$ (Fig. 15), and $\kappa - N_{\text{MI}}$ (Fig. 16) plane. The conventions adopted for the various lines are displayed in the r.h.s of every graph. In particular, the black solid [dashed] lines correspond to $n_s = 0.99$ [$n_s = 0.926$] whereas the gray solid lines have been obtained by fixing $n_s = 0.958$ – see Eq. (1). The dot-dashed [double dot-dashed] lines correspond to the lower bound on $V_{\text{HI}0}$ [N_{MI}] from Eq. (50) [Eq. (49)]. The bold [faint] dotted lines correspond to $\alpha_s = -0.01$ [$\alpha_s = -0.005$]. Let us notice that:
 - The resulting v_G 's and κ 's are restricted to rather large values (although $v_G < M_{\text{GUT}}$) compared to those allowed within the other scenaria with one inflationary epoch (compare with Figs. 5 and 8). As a consequence, the SUGRA corrections in Eq. (10) play an important role.
 - The lower bound on $V_{\text{HI}0}$ from Eq. (50) cut out sizeable slices of the allowed regions presented in Ref. [22]. This is due to the fact that we take here a much larger m_s in order to fulfill Eq. (59) – not considered in Ref. [22].
 - The requirement of Eq. (47) does not constrain the parameters since it is overshadowed by the constraint of Eq. (50).
 - In almost the half of the available parameter space for $n_s \sim 0.958$ we have relatively high $|\alpha_s|$, $0.005 \lesssim |\alpha_s| \lesssim 0.01$.
 - For $n_s = 0.958$, we obtain $0.04 \lesssim \kappa \lesssim 0.14$, $0.89 \lesssim v_G/(10^{16} \text{ GeV}) \lesssim 1.08$ and $0.003 \lesssim |\alpha_s| \lesssim 0.01$. Also, $12 \lesssim N_{\text{HI}^*} \lesssim 21.7$, $35 \gtrsim N_{\text{MI}} \gtrsim 28$ and $0.64 \lesssim m_s/H_s \lesssim 0.74$. So, the interesting solutions correspond to slow rather than fast-roll MI.
- **Shifted FHI.** We list input and output parameters consistent with Eqs. (19), (44), (47) – (50), (54) and (59) for the nearest to M_{GUT} v_G and selected n_s 's in Table 4. The values of v_G come out considerably larger than in the case of standard FHI. However, the satisfaction of Eq. (50) in conjunction with Eq. (59) leads to $v_G > M_{\text{GUT}}$. Indeed, $v_G = M_{\text{GUT}}$ occurs for low κ 's which produce $V_{\text{HI}0}$'s inconsistent with Eq. (50) – compare with Ref. [22].
- **Smooth FHI.** We arrange input and output parameters consistent with Eqs. (19), (44), (47) – (50), (54) and (59) for $v_G = M_{\text{GUT}}$ and selected n_s 's in Table 4. In contrast with standard and shifted FHI, we can achieve $v_G = M_{\text{GUT}}$ for every n_s in the range of Eq. (1). The mSUGRA corrections in Eq. (10) play an important role for every M_S encountered in Table 4 and $|\alpha_s|$ is considerably enhanced but compatible with Eq. (48).

(ii) If s acquires mass, s_{MI} can be evaluated from Eq. (53). However, due to our ignorance of N_{HI} , there is an uncertainty in the determination of m_s/H_s , i.e. for every N_{MI} required by Eq. (44), we can derive a maximal [minimal], $m_s/H_s|_{\text{max}}$ [$m_s/H_s|_{\text{min}}$], value

SHIFTED FHI				SMOOTH FHI			
n_s	0.926	0.958	0.99	n_s	0.926	0.958	0.99
$v_G/10^{16}$ GeV	5.86	6.4	6.91	$v_G/10^{16}$ GeV	2.86	2.86	2.86
κ	0.035	0.04	0.045	$M_S/5 \times 10^{17}$ GeV	0.815	0.87	0.912
$\sigma_*/10^{16}$ GeV	6.97	11.3	20.15	$\sigma_*/10^{16}$ GeV	22.18	23.53	25.54
$M/10^{16}$ GeV	4.57	4.92	5.24	$\mu_S/10^{16}$ GeV	0.2	0.188	0.179
$1/\xi$	4.2	4.13	4.09	$\sigma_f/10^{16}$ GeV	13.43	13.43	13.43
$N_{\text{HI}*}$	12.75	20.8	40.45	$N_{\text{HI}*}$	13.6	18	26
$-\alpha_s/10^{-3}$	6	2.5	1	$-\alpha_s/10^{-3}$	9	5.5	3
N_{MI}	31.1	23.1	3.35	N_{MI}	30.3	25.6	17.8
m_s/H_s	0.68	0.8	2.45	m_s/H_s	0.69	0.75	0.92

TABLE 4: Input and output parameters consistent with Eqs. (19), (44), (47) – (50), (54) and (59) in the cases of shifted ($M_S = 5 \times 10^{17}$ GeV) or smooth FHI for $s_{\text{MI}}/m_{\text{P}} = 0.01$, the nearest to $M_{\text{GUT}} v_G$ and selected n_s 's within the mSUGRA double inflationary scenario when the inflaton of MI does not acquire effective mass.

of m_s/H_s . Eq. (60) implies that $m_s/H_s|_{\text{max}} [m_s/H_s|_{\text{min}}]$ is obtained by using the minimal [maximal] possible value of s_{MI} which corresponds to $N_{\text{HI}} = N_{\text{HI}}^{\text{max}} [N_{\text{HI}} = N_{\text{HI}*}]$. Our results are presented in Figs. 17 – 20 for standard FHI (with $N = 2$) and in Table 5 for shifted and smooth FHI. Let us discuss each case separately:

- **Standard FHI.** We present the regions allowed by Eqs. (1), (19), (44) and (47) – (49), (57) and (59) in the $\kappa - v_G$ (Fig. 17), $\kappa - m_s/H_s$ (Fig. 18), $\kappa - N_{\text{HI}*}$ (Fig. 19), and $\kappa - N_{\text{MI}}$ (Fig. 20) plane. The conventions adopted for the various lines are displayed in the r.h.s of every graph. In particular, the black solid [dashed] lines correspond to $n_s = 0.99$ [$n_s = 0.926$] whereas the gray solid lines have been obtained by fixing $n_s = 0.958$ – see Eq. (1). The dot-dashed [double dot-dashed] lines correspond to the lower [upper] bound on $N_{\text{HI}*}$ from Eq. (47) [Eq. (57)]. The double dot-dashed lines correspond to the upper [lower] bound on m_s/H_s [N_{MI}] from Eq. (36) [Eq. (49)]. The bold [faint] dotted lines correspond to $\alpha_s = -0.01$ [$\alpha_s = -0.005$]. Let us notice that:
 - Lower than those seen in Fig. 13 (but still larger than those shown in Figs. 5 and 8) v_G 's and κ 's are allowed in Fig. 17, since the constraint of Eq. (50) is not applied here. As κ increases above 0.01 the mSUGRA corrections in Eq. (10) become more and more significant.
 - The constraint from the upper bound on N_{HI} in Eq. (57) is very restrictive and almost overshadows this from the lower bound on N_{MI} in Eq. (49) (which is applied, e.g., only in the upper left corner of the allowed region in Fig. 18).
 - In contrast with the case (i), $0.005 \lesssim |\alpha_s| \lesssim 0.01$ holds only in a very limited part of the allowed regions.

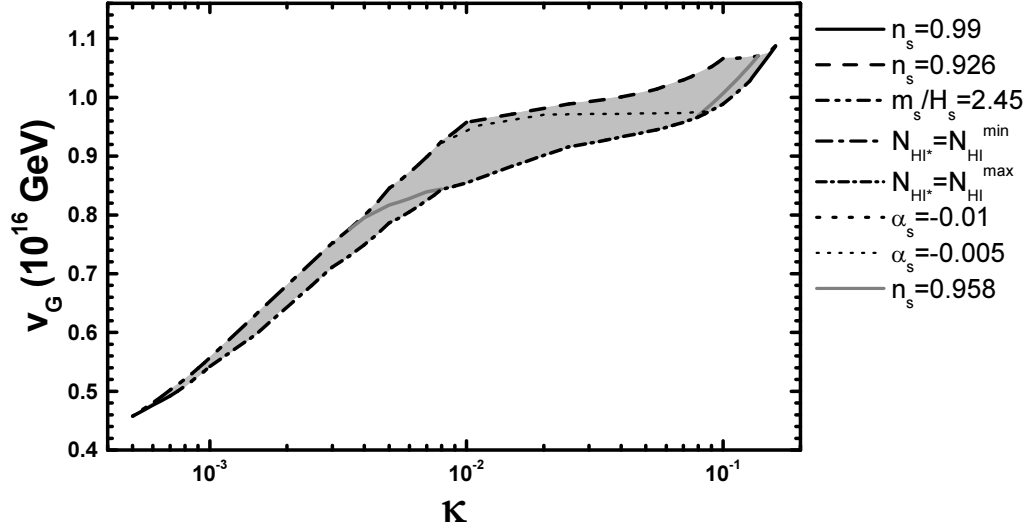


FIGURE 17: Allowed (lightly gray shaded) region in the $\kappa - v_G$ plane for standard FHI followed by MI realized by a field which acquires effective mass before MI. The conventions adopted for the various lines are also shown.

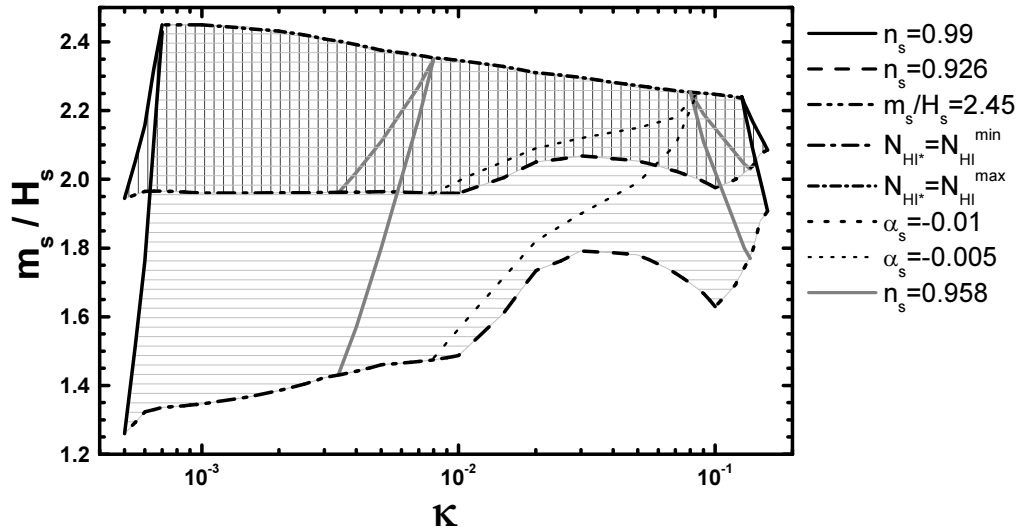


FIGURE 18: Allowed regions in the $\kappa - m_s/H_s$ plane for $N_{\text{HI}} = N_{\text{HI}}^{\text{max}}$ (dark gray ruled region) or $N_{\text{HI}} = N_{\text{HI}^*}$ (lightly gray ruled region) and standard FHI followed by MI realized by a field which acquires effective mass before MI. The conventions adopted for the various lines are also shown.

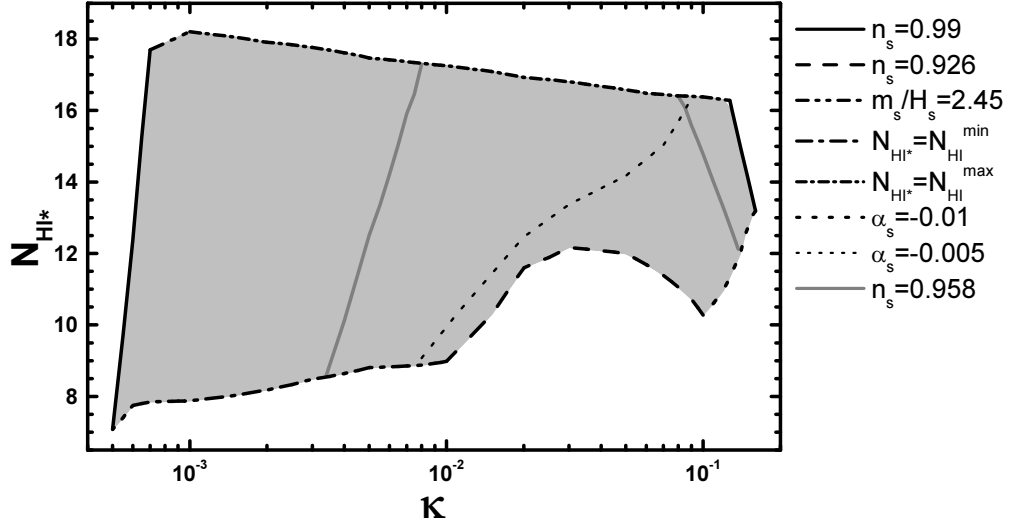


FIGURE 19: Allowed (lightly gray shaded) region in the $\kappa - N_{\text{HI}^*}$ plane for standard FHI followed by MI realized by a field which acquires effective mass before MI. The conventions adopted for the various lines are also shown.

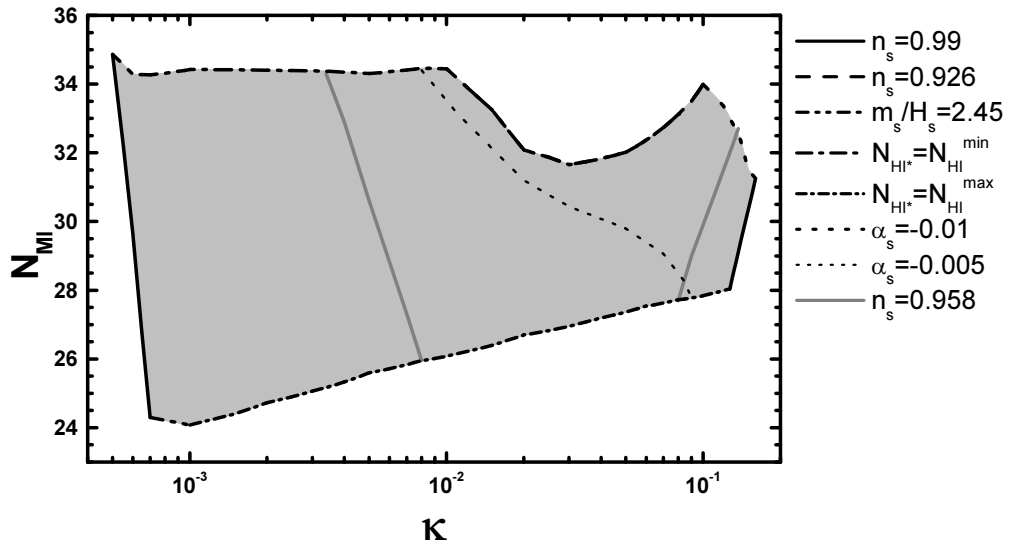


FIGURE 20: Allowed (lightly gray shaded) region in the $\kappa - N_{\text{MI}}$ plane for standard FHI followed by MI realized by a field which acquires effective mass before MI. The conventions adopted for the various lines are also shown.

SHIFTED FHI				SMOOTH FHI			
n_s	0.926	0.958	0.99	n_s	0.926	0.958	0.99
$v_G/10^{16}$ GeV	2.86	1.93	12	$v_G/10^{16}$ GeV	2.86	3.3	4.61
κ	0.0106	0.0055	0.13	$M_S/5 \times 10^{17}$ GeV	0.815	1.06	1.66
$\sigma_*/10^{16}$ GeV	2.23	1.82	28.9	$\sigma_*/10^{16}$ GeV	22.18	25.73	32.8
$M/10^{16}$ GeV	2.38	1.65	8.95	$\mu_S/10^{16}$ GeV	0.2	0.21	0.25
$1/\xi$	4.67	5.04	4.05	$\sigma_f/10^{16}$ GeV	13.43	14.8	18.4
N_{HI^*}	10.85	17.1	16.3	N_{HI^*}	13.6	16.6	16.5
$-\alpha_s/10^{-3}$	5.6	1.9	7.3	$-\alpha_s/10^{-3}$	9	6.7	7.6
N_{MI}	32.6	26	28	N_{MI}	30.3	27.4	27.6
$m_s/H_s _{\text{max}}$	2.03	2.3	2.45	$m_s/H_s _{\text{max}}$	2.12	2.3	2.3
$m_s/H_s _{\text{min}}$	1.6	2.3	2.45	$m_s/H_s _{\text{min}}$	1.94	2.3	2.3

TABLE 5: Input and output parameters consistent with Eqs. (19), (44) and (47) – (49), (57) and (59) in the cases of shifted ($M_S = 5 \times 10^{17}$ GeV) or smooth FHI for the nearest to $M_{\text{GUT}} v_G$ and selected n_s 's within the mSUGRA double inflationary scenario when the inflaton of MI acquires effective mass before MI.

– For $n_s = 0.958$, we obtain $0.0035 \lesssim \kappa \lesssim 0.0085$ and $0.77 \lesssim v_G/(10^{16} \text{ GeV}) \lesssim 0.85$, or $0.08 \lesssim \kappa \lesssim 0.14$ and $0.96 \lesssim v_G/(10^{16} \text{ GeV}) \lesssim 1.08$. Also $0.002 \lesssim |\alpha_s| \lesssim 0.01$, $8.5 \lesssim N_{\text{HI}^*} \lesssim 17.3$, $34.3 \gtrsim N_{\text{MI}} \gtrsim 26$ and $(1.4 - 1.96) \lesssim m_s/H_s \lesssim 2.35$. So, the interesting solutions correspond to fast rather than slow-roll MI.

- **Shifted FHI.** We list input and output parameters consistent with Eqs. (19), (44) and (47) – (49), (57) and (59) for the nearest to $M_{\text{GUT}} v_G$ and selected n_s 's in Table 5. The values of v_G come out again considerably larger than in the case of standard FHI. However, we take $v_G = M_{\text{GUT}}$ only for $n_s = 0.926$ since the satisfaction of Eq. (57) requires $v_G < M_{\text{GUT}}$ [$v_G > M_{\text{GUT}}$] for $n_s = 0.958$ [$n_s = 0.99$]. The closest to M_{GUT} values of v_G for $n_s = 0.958$ and 0.99 are attained for $N_{\text{HI}^*} = N_{\text{HI}}^{\text{max}}$ and so, $m_s/H_s|_{\text{min}} = m_s/H_s|_{\text{max}}$.
- **Smooth FHI.** We display input and output parameters consistent with Eqs. (19), (44) and (47) – (49), (57) and (59) for the nearest to $M_{\text{GUT}} v_G$ and selected n_s 's in the Table 5. The results are quite similar to those for shifted FHI except for the fact that we have $v_G > M_{\text{GUT}}$ for $n_s = 0.958$ and 0.99 and that $|\alpha_s|$ remains considerably enhanced.

5 CONCLUSIONS

We reviewed the basic types (standard, shifted and smooth) of FHI in which the GUT breaking v.e.v, v_G , turns out to be comparable to SUSY GUT scale, M_{GUT} . Indeed, confronting these models with the restrictions on $P_{\mathcal{R}*}$ we obtain that v_G turns out a little lower than M_{GUT} for standard FHI whereas $v_G = M_{\text{GUT}}$ is possible for shifted and smooth FHI. However, the predicted n_s is just marginally consistent with the fitting of the WMAP3 data by the standard power-law Λ CDM cosmological model – if the horizon and flatness problems of SBB are resolved exclusively by FHI.

We showed that the results on n_s can be reconciled with data if we consider one of the following scenaria:

(i) FHI within qSUGRA. In this case, acceptable n_s 's can be obtained by appropriately restricting the parameter c_q involved in the quasi-canonical Kähler potential, with a convenient sign. We paid special attention to the monotonicity of the inflationary potential which is crucial for the safe realization of FHI. Enforcing the monotonicity constraint, reduction of n_s below around 0.95 is prevented. Fixing in addition n_s to its central value, we found that (i) relatively large κ 's but rather low v_G 's are required within standard FHI with $0.013 \lesssim c_q \lesssim 0.03$ and (ii) $v_G = M_{\text{GUT}}$ is possible within smooth FHI with $c_q \simeq 0.0083$ but not within shifted FHI.

(ii) FHI followed by MI. In this case, acceptable n_s 's can be obtained by appropriately restricting the number of e-foldings $N_{\text{HI}*}$. A residual number of e-foldings is produced by a bout of MI realized at an intermediate scale by a string modulus. We have taken into account extra restrictions on the parameters originating from:

- The resolution of the horizon and flatness problems of SBB.
- The requirements that FHI lasts long enough to generate the observed primordial fluctuations on all the cosmological scales and that these scales are not reprocessed by the subsequent MI.
- The limit on the running of n_s .
- The naturalness of MI.
- The homogeneity of the present universe.
- The complete randomization of the modulus if this remains massless before MI or its evolution before MI if it acquires effective mass.
- The establishment of RD before the onset of NS.

We discriminated two basic versions of this scenario, depending whether the modulus does or does not acquire effective mass before MI. We concluded that:

- If the modulus remains massless before MI, the combination of the randomization and NS constraints pushes the values of the inflationary plateau to relatively large values. Fixing n_s to its central value, we got (i) $v_G < M_{\text{GUT}}$ and $10 \lesssim N_{\text{HI}^*} \lesssim 21.7$ within the standard FHI, (ii) $v_G > M_{\text{GUT}}$ and $N_{\text{HI}^*} \simeq 21$ within shifted FHI and (iii) $v_G = M_{\text{GUT}}$ and $N_{\text{HI}^*} \simeq 18$ within smooth FHI. In all cases, MI of the slow-roll type, with $m_s/H_s \sim (0.6 - 0.8)$, and a mild (of the order of 0.01) tuning of the initial value of the modulus produces the necessary additional number of e-foldings.
- If the modulus acquires effective mass before MI, lower values, than those encountered in the case (i), of the inflationary plateau are available. Fixing n_s to its central value, we got (i) $v_G < M_{\text{GUT}}$ and $8.5 \lesssim N_{\text{HI}^*} \lesssim 17.5$ within the standard FHI and (ii) $v_G < M_{\text{GUT}}$ [$v_G > M_{\text{GUT}}$] and $N_{\text{HI}^*} \simeq 17$ within shifted [smooth] FHI. In all cases, MI of the fast-roll type with $m_s/H_s \sim (1.4 - 2.45)$ and without any tuning of the initial value of the modulus produces the necessary additional number of e-foldings. However, FHI is constrained to be of short duration, producing a total number of e-foldings, $N_{\text{HI}} \lesssim 17$. This is rather questionable and can be evaded by introducing a more elaborated structure for the Kähler potential or superpotential of the modulus (see, e.g., Ref. [34, 41]).

Trying to compare the proposed methods for the reduction of n_s within FHI, we can do the following comments:

- The main advantage of the method in the case (i) is that the standard one-step inflationary cosmological set-up remains intact. This method becomes rather attractive when the minimum-maximum structure of the inflationary potential is avoided. However, the possible in this way decrease of n_s is rather limited.
- The method of the case (ii) offers a comfortable reduction of n_s but it requires a more complicate cosmological set-up with advantages (dilution of gravitinos and defects) and disadvantages (complications with baryogenesis). The most natural and simple version of this scenario is realized when the modulus remains massless during FHI since it requires a very mild tuning.

Hopefully, the proposed scenaria will be further probed by the measurements of the Planck satellite which is expected to give results on n_s with an accuracy $\Delta n_s \simeq 0.01$ by the end of the decade [46].

Acknowledgments

We would like to thank G. Lazarides and A. Pilaftsis for fruitful and pleasant collaborations, from which parts of this work are culled. This work was supported from the PPARC research grant PP/C504286/1.

REFERENCES

- [1] A.H. Guth, Phys. Rev. D **23**, 347 (1981).
- [2] D.H. Lyth and A. Riotto, Phys. Rept. **314**, 1 (1999) [hep-ph/9807278].
- [3] G. Lazarides, Lect. Notes Phys. **592**, 351 (2002) [hep-ph/0111328];
G. Lazarides, J. Phys. Conf. Ser. **53**, 528 (2006) [hep-ph/0607032].
- [4] A. Riotto, hep-ph/0210162.
- [5] G. Lazarides, hep-ph/0011130.
- [6] E.J. Copeland *et al.*, Phys. Rev. D **49**, 6410 (1994) [astro-ph/9401011].
- [7] G.R. Dvali, Q. Shafi and R.K. Schaefer, Phys. Rev. Lett. **73**, 1886 (1994) [hep-ph/9406319];
G. Lazarides, R.K. Schaefer, and Q. Shafi, Phys. Rev. D **56**, 1324 (1997) [hep-ph/9608256].
- [8] R. Jeannerot *et al.*, J. High Energy Phys. **10**, 012 (2000) [hep-ph/0002151].
- [9] G. Lazarides and C. Panagiotakopoulos, Phys. Rev. D **52**, 559 (1995) [hep-ph/9506325];
G. Lazarides *et al.*, Phys. Rev. D **54**, 1369 (1996) [hep-ph/9606297];
R. Jeannerot, S. Khalil, and G. Lazarides, Phys. Lett. B **506**, 344 (2001) [hep-ph/0103229].
- [10] A.D. Linde and A. Riotto Phys. Rev. D **56**, 1841 (1997) [hep-ph/9703209];
V.N. Şenoğuz and Q. Shafi, Phys. Lett. B **567**, 79 (2003) [hep-ph/0305089].
- [11] D.N. Spergel *et al.*, Astrophys. J. Suppl. **170**, 377 (2007) [astro-ph/0603449];
<http://lambda.gsfc.nasa.gov/product/map/dr2/parameters.cfm>
- [12] R.A. Battye *et al.*, J. Cosmol. Astropart. Phys. **09**, 007 (2006) [astro-ph/0607339].
- [13] G. Lazarides *et al.*, Phys. Rev. D **70**, 123527 (2005) [hep-ph/0409335].
- [14] R. Jeannerot and M. Postma, J. High Energy Phys. **05**, 071 (2005) [hep-ph/0503146].
- [15] J. Rocher and M. Sakellariadou, J. Cosmol. Astropart. Phys. **03**, 004 (2005) [hep-ph/0406120].
- [16] B. Garbrecht *et al.*, J. High Energy Phys. **12**, 038 (2006) [hep-ph/0605264].
- [17] M. Bastero-Gil, S.F. King, and Q. Shafi, Phys. Lett. B **651**, 345 (2007) [hep-ph/0604198].
- [18] C. Panagiotakopoulos, Phys. Lett. B **402**, 257 (1997) [hep-ph/9703443].
- [19] L. Boubekeur and D. Lyth, J. Cosmol. Astropart. Phys. **07**, 010 (2005) [hep-ph/0502047].
- [20] M.ur Rehman, V.N. Şenoğuz, and Q. Shafi, Phys. Rev. D **75**, 043522 (2007) [hep-ph/0612023].
- [21] G. Lazarides and A. Vamvasakis, arXiv:0705.3786.
- [22] G. Lazarides and C. Pallis, Phys. Lett. B **651**, 216 (2006) [hep-ph/0702260];
G. Lazarides, arXiv:0706.1436.
- [23] P. Binétruy and M.K. Gaillard, Phys. Rev. D **34**, 3069 (1986);
F.C. Adams *et al.*, Phys. Rev. D **47**, 426 (1993) [hep-ph/9207245];
T. Banks *et al.*, Phys. Rev. D **52**, 3548 (1995) [hep-ph/9503114];
R. Brustein *et al.*, Phys. Rev. D **68**, 023517 (2003) [hep-ph/0205042].

- [24] G. Lazarides and A. Vamvasakis, arXiv:0709.3362.
- [25] M. Dine, L. Randall and S. Thomas, Phys. Rev. Lett. **75**, 398 (1995) [hep-ph/9503303];
M.K. Gaillard, H. Murayama and K.A. Olive, Phys. Lett. B **355**, 71 (1995) [hep-ph/9504307].
- [26] D.H. Lyth and T. Moroi, J. High Energy Phys. **05**, 004 (2004) [hep-ph/0402174].
- [27] A. Linde, J. High Energy Phys. **11**, 052 (2001) [hep-ph/0110195].
- [28] G. Dvali, hep-ph/9503259.
- [29] M.Yu. Khlopov and A.D. Linde, Phys. Lett. B **138**, 265 (1984);
J. Ellis, J.E. Kim, and D.V. Nanopoulos, *ibid.* **145**, 181 (1984).
- [30] T.W.B. Kibble, J. Phys. A **9**, 387 (1976).
- [31] G. Ballesteros *et al.*, J. Cosmol. Astropart. Phys. **03**, 001 (2006) [hep-ph/0601134].
- [32] V.N. Şenoğuz and Q. Shafi, Phys. Rev. D **71**, 043514 (2005) [hep-ph/0412102].
- [33] D.H. Lyth and D. Wands, Phys. Lett. B **524**, 5 (2002) [hep-ph/0110002];
T. Moroi and T. Takahashi, Phys. Lett. B **522** 215 (2001);
T. Moroi and T. Takahashi, Phys. Lett. B **539** 303(E) (2002) [hep-ph/0110096];
D. H. Lyth, C. Ungarelli and D. Wands, Phys. Rev. D **67** 023503 (2003) [astro-ph/0208055].
- [34] M. Kawasaki *et al.*, Phys. Rev. D **68**, 023508 (2003) [hep-ph/0304161];
M. Yamaguchi and J. Yokoyama, Phys. Rev. D **68**, 123520 (2003) [hep-ph/0307373];
M. Yamaguchi and J. Yokoyama, Phys. Rev. D **70**, 023513 (2004) [hep-ph/0402282];
M. Kawasaki *et al.*, Phys. Rev. D **74**, 043525 (2006) [hep-ph/0605271].
- [35] J. Garcia-Bellido *et al.*, Phys. Rev. D **60**, 123504 (1999) [hep-ph/9902449];
L.M. Krauss and M. Trodden, Phys. Rev. Lett. **83**, 1502 (1999) [hep-ph/9902420].
- [36] K. Benakli and S. Davidson, Phys. Rev. D **60**, 025004 (1999) [hep-ph/9810280].
- [37] G. Dvali and S. Kachru, hep-ph/0310244.
- [38] C.P. Burgess *et al.*, J. High Energy Phys. **05**, 067 (2005) [hep-th/0501125].
- [39] U. Seljak, *et al.*, J. Cosmol. Astropart. Phys. **10**, 014 (2006) [astro-ph/0604335].
- [40] A.A. Starobinsky and J. Yokoyama, Phys. Rev. D **50**, 6357 (1994);
E.J. Chun, K. Dimopoulos and D. Lyth, Phys. Rev. D **70**, 103510 (2004) [hep-ph/0402059].
- [41] K.I. Izawa, M. Kawasaki, and T. Yanagida, Phys. Lett. B **411**, 249 (1997) [hep-ph/9707201];
M. Kawasaki, N. Sugiyama, and T. Yanagida, Phys. Rev. D **57**, 6050 (1998) [hep-ph/9710259];
M. Kawasaki and T. Yanagida, Phys. Rev. D **59**, 043512 (1999) [hep-ph/9807544].
- [42] G.D. Coughlan, W. Fischler, E. Kolb, S. Raby and G.G. Ross, Phys. Lett. B **131** (1983) 59;
B. de Carlos *et al.*, Phys. Lett. B **318**, 447 (1993) [hep-ph/9308325].
- [43] M. Berkooz, M. Dine and T. Volansky, Phys. Rev. D **71** 103502 (2005) [hep-ph/0409226].
- [44] M. Endo *et al.*, Phys. Rev. Lett. **96**, 211301 (2006) [hep-ph/0602061];
S. Nakamura and M. Yamaguchi, Phys. Lett. B **638**, 389 (2006) [hep-ph/0602081].
- [45] C. Pallis, Nucl. Phys. **B751**, 129 (2006) [hep-ph/0510234].
- [46] <http://www.rssd.esa.int/SA/PLANCK/include/report/redbook/redbook-science.htm>